Praise Worthy Prize

International Review of Chemical Engineering (I.RE.CH.E.), Vol. 4, N. 1
ISSN 2035-1755 *January 2012*

Fluidization of Ultrafine Powders

INVITED PAPER

Jaber Shabanian, Rouzbeh Jafari, Jamal Chaouki

Abstract – *Due to their unique properties arising from their very small primary particle size and very large surface area per unit mass, ultrafine powders are applied in a wide range of processes and their application continues to increase. Gas fluidization is one the best techniques available for dispersing and processing these particles. However, they cannot be fluidized separately and, in fact, tend to fluidize as large sized very porous aggregates. In order to achieve a proper fluidization, appropriate assisting method is required. This contribution reviews experimental and theoretical studies on gas fluidization of ultrafine particles. It includes introduction of different forces playing role on the fluidization of these powders, phenomenological discussion on how they can be fluidized, a summary of various assisting methods and their impacts for improving the fluidization quality of these powders, a summary of different experimental methods for measuring the agglomerate size followed by different modeling approaches for the prediction of this important parameter, a brief review on different applications of these particles and their bed expansion behavior. With respect to the current and upcoming applications of ultrafine powders in industrial sectors, considerable theoretical and experimental work is left for mining new opportunities in chemical engineering on the subject of fluidization of ultrafine particles.*

Keywords: *Fluidization, Fine and Ultrafine Powders, Nanoparticles*

Nomenclature

A_e	Agglomerate number
A_m	Vibration amplitude, m
Bo_g	Granular Bond number
$Bo_g{}^*$	Granular Bond number of simple agglomerate
C_a	Parameter used for definition of E_a, J/kg
C_D	Drag coefficient
d_a	Agglomerate size, m
d_p	Particle size, m
d^*	Simple agglomerate size, m
d^{**}	Complex agglomerate size, m
D_a	Fractal dimension
D_b	Bubble diameter, m
D_{col}	Column diameter, m
D^*	Fractal dimension of the complex agglomerates
E_a	Attainable energy, J/kg
E_{break}	Energy required to break an agglomerate, J
E_{coh}	Cohesion energy, J
E_{coll}	Collision energy, J
E_{dw}	Agglomerate disruption energy per unit weight of agglomerate, J/kg
E_{ext}	Energy given to the system by external field, J
E_{vib}	Vibration energy, J
E_{sou}	Sound wave energy, J
f_s	Sound frequency, Hz
f_{sc}	Critical sound frequency, Hz
f_v	Vibration frequency, Hz
F_b	Buoyant force, N
F_c	Capillary force, N
F_d	Drag force, N
F_e	Electrostatic force, N
F_{IPF}	Interparticle attractive force, N
F_p	Force due to pressure difference across the air-liquid interface, N
F_s	Shear force, N
F_{vdw}	Van der Waals force, N
F_γ	Surface tension force, N
F^*	Interparticle attractive force between simple agglomerates, N
Fr_{mf}	Froude number at u_{mf}
g	Gravity field acceleration, m/s^2
g_{ef}	Effective acceleration, m/s^2
H	Bed height, m
H_a	Hamaker constant, J
H_{mf}	Bed height at u_{mf}, m
H_r	Hardness, N/m^2
H_0	Fixed bed height, m
$h\bar{\omega}$	Liftshits-van der Waals coefficient, J
k	Function of Poisson's ration and Young's modulus, Pa^{-1}
k_a	Ratio of agglomerate size to particle size
k_{at}	Sound attenuation coefficient, s
k^*	Ratio of complex agglomerate size to simple agglomerate size
K_c	Agglomerate spring constant

Manuscript received and revised December 2011, accepted January 2012

m_p	Particle mass, kg
n	Richardson-Zaki exponent
$n_{k,mf}$	Coordinate number of agglomerates at u_{mf}
N_a	Number of particles in an agglomerate
N_s	Number of primary nanoparticles in a simple agglomerate
N^*	Number of simple agglomerates in a complex agglomerate
P_s	Dimensionless particle pressure
$\overline{P_{s,n}}$	Dimensionless average particle pressure of non-sticky system
q_i	Charges carried by objects, i = 1,2, C
R	Particle radius, m
R_a	Agglomerate radius, m
R_{as}	Particle asperity radius, m
Re_{mf}	Reynolds number at u_{mf}
Re_p	Particle Reynolds number
Re_t	Terminal velocity Reynolds number
s	Distance between two objects, m
u_{mf}	Agglomerate minimum fluidization velocity, m/s
u_{p0}	Terminal velocity of a single particle, m/s
$u_{p0}{}^*$	Velocity extrapolated from Eq. (52) at $\varepsilon = 1$, m/s
u_s	Initial settling velocity, m/s
u_{tsa}	Terminal settling velocity of agglomerate, m/s
u_0	Superficial gas velocity, m/s
u_{0l}	Superficial liquid velocity, m/s
V	Relative velocity of agglomerates, m/s
W_b	Buoyant weight, N
Z	Separation distance between particles, m

Greek letters

α	Half-filling angle
β	Contact angle
γ	Liquid-surface tension, N/m
γ_s	Agglomerate spring strain, N/m
ε	Bed voidage
ε_a	Agglomerate voidage
ε_0	Fixed bed voidage
ϵ	Permittivity of the surrounding, F/m
θ	Elasticity exponent
μ	Fluid viscosity, Pa s
ξ	Interparticle attractive force constant
ρ_a	Agglomerate density, kg/m^3
ρ_{a0}	Agglomerate density before fluidization, kg/m^3
ρ_b	Aerated bulk density of primary particles,
ρ_e	Density of emulsion phase in fluidized bed, kg/m^3
ρ_f	Fluid density, kg/m^3
ρ_{fb}	Density of fluidized bed, kg/m^3
ρ_p	Particle density, kg/m^3
ρ_{tb}	Tapped bulk density, kg/m^3
σ	Maximum tensile strength of agglomerate, Pa
ϕ	Particle volume fraction
ϕ_a	Agglomerate volume fraction
Γ	Vibration intensity
Δp	Differential pressure across air-liquid interface, Pa
Λ	Ratio of effective acceleration to gravity field acceleration

Acronyms

ABF	Agglomerate Bubbling Fluidization
APF	Agglomerate Particulate Fluidization
MSA	Multi-stage agglomerate
SPL	Sound Pressure Level
SPL_c	Critical Sound Pressure Level
SPL_{min}	Minimum Sound Pressure Level
SSA	Single-stage agglomerate

I. Introduction

Fine powders, including ultrafine or nano size powders, play a moderate role and will be highly important in industrial applications. Processing these powders is very attractive due to their very small primary size and large surface area-to-volume ratio [1], [2], because as in the case of gas/solid and solid/solid reactions, for example, higher reaction rates per unit volume of reactor are obtainable [3]. Nanoparticles have been used to produce catalysts, effective sorbents, drugs, cosmetics, food, plastics, biomaterials, and microelectro-mechanical systems (MEMS). In addition, they have some applications in hydrogen storage, Li-ion batteries, and fuel cells [1], [4], [5].

Therefore, it is essential to develop processing technologies that can handle large quantities of nano size particles, such as mixing, transporting, and modifying the surface properties, and to produce nanocomposities [1].

Prior to processing such materials, however, it is necessary that the nanopowders be well dispersed. Gas fluidization is one of the best techniques available to disperse and process fine particles [1], [4]. Gas-solid fluidized beds are among the unit operations, which have a number of significant advantages for processing small solid particles, including high heat and mass transfer rates, uniform and controllable bed temperature, high flowability of particles, the ability to handle a wide variety of particle properties and suitability for large-scale operations [6]-[8].

Moreover, compared to liquid-phase processing of nanoparticles, gas-phase processing reduces difficulties that arise with respect to removing impurities and drying the particles, and allows easier scale-up [4], [9].

Geldart [10] classified powders according to their primary particle size and density into four distinct groups: A, aeratable; B, sand-like; C, cohesive; and D, spoutable. On the basis of their physical properties, nano size powders fall under the Geldart group C (<30 μm) classification [11].

It has been believed that group C powders are in principle extremely hard to fluidize and, hence, can be difficult for practical use in their original separated form,

not only due to the fact that the cohesive forces (such as van der Waals, electrostatic, capillary forces) in these powders are much larger than the gravitational, but also because the drag force exerted by the gas on these particles is not large enough for fluidization [12], [13]. Unlike group A and B powders, fluidization of this group of materials generally results in gas bypassing via the formation of channels and in low powder mobility. The presence of channeling in the bed gives rise to some undesirable effects, such as low bed expansion, inadequate bed pressure drop, and the creation of regions with high local gas velocities, causing undesired elutriation loss of expensive bed materials [14].

However, despite Geldart classification, there is growing experimental evidence that nanoparticles can be fluidized via the formation of agglomerates of original ultrafine particles at gas velocities in excess of the minimum fluidization for the primary particle [12], [15]-[20]. This implies that primary particle size and density cannot be taken as representative parameters for predicting their fluidization behavior [17], [20]. In fact, because of strong interparticle forces, nanoparticles are mainly found to be in the form of large-size (100-400μm), highly porous (internal porosity>98%), fractal structured agglomerates of primary particles, rather than as isolated particles when they are subjected to gas fluidization. Therefore, gas fluidization of ultrafine powders actually refers to the fluidization of nanoparticle agglomerates and their properties (size, density, structure, etc.) highly affect the fluidization nature [1], [19]-[22].

Accordingly, it is very important to know how these agglomerate particles fluidize within the bed. In fact, fluidization behavior of highly porous agglomerates can be categorized into two distinct paths: *agglomerate particulate fluidization* (APF) and *agglomerate bubbling fluidization* (ABF). The former is characterized by very large bed expansion, homogeneous fluidization, and very low minimum fluidization velocity; the latter, instead, shows little bed expansion, high minimum fluidization velocity, and bubbling [1], [19], [20], [22].

Fluidization of nanoparticle agglomerates suffers from several problems, such as channeling, bubbling, clustering, and elutriation. As a consequence, inappropriate dispersion of nanoparticles in the gas phase and considerable gas bypassing may occur [4]. To overcome these problems and improve the fluidization quality of nanoparticle agglomerates, various assisting methods have been proposed and tested. These methods include the application of additional generated forces, for example by acoustic [23]-[27], electric [28], [29], or magnetic [30], [31] fields, or mechanical vibrations [32], [33], the use of a centrifugal fluidized bed [2], [7], [34], [35], the use of a tapered fluidized bed [36], the addition of foreign particles [12], [37], [38], and the use of micro-jets as a secondary flow in the bed [22]. The degree of fluidization enhancement achieved by applying these methods is evaluated by measuring some hydrodynamic parameters, such as minimum fluidization velocity, bed pressure drop, bed expansion, agglomerate size, degree of mixing, bubble suppression and the amount of powder elutriation, as indicators of fluidization quality.

In this chapter the studies done on the fluidization of ultrafine powders will be reviewed. Firstly, different forces that directly or indirectly affect the dynamics of the fluidized bed will be introduced and correlations for the prediction of their magnitudes will be reported. Secondly, the fluidization behavior of all powders falling into Geldart group C category is phenomenologically discussed. Thirdly, a summary of different assisting methods and their impacts for enhancing the fluidization quality of fine/ultrafine particles will be provided. Then, different experimental techniques that have been used for measuring agglomerate size will be introduced. Section six is devoted to the presentation of different modeling approaches for the prediction of agglomerate size. Different applications of ultrafine particles will be reviewed in section seven. Next, expansion behavior of the bed of fine/ultrafine particles will be discussed. Finally, a brief summary of the article will be presented.

II. Various Forces in a Gas-Solid Fluidized Bed

In gas-solid flows, forces controlling the motions of particles can be categorized into three groups: (1) forces through the interface between particles and fluid, (2) forces imposed by external fields, and (3) forces due to the interactions between particles, interparticle forces. Although field and interparticle forces do not have a direct impact on the flow pattern in the bed, they may indirectly affect the fluid motion via particle-fluid interactions [39]. In conventional gravity driven gas-solid fluidized beds drag force, buoyant weight, and interparticle forces influence the motion of gas-solid flow. Each of these forces will be separately delineated below.

II.1. Drag Force

The drag force F_d on a single isolated particle, with particle diameter d_p, in a uniform flow field considering superficial gas velocity u_0 and drag coefficient C_D, can be generally given by:

$$F_d = C_D \frac{\pi {d_p}^2}{4} \frac{\rho_f {u_0}^2}{2} \quad (1)$$

The drag coefficient is a function of the particle Reynolds number, Re_p, which is defined as:

$$Re_p = \frac{\rho_f u_o d_p}{\mu} \quad (2)$$

where ρ_f and μ are fluid density and viscosity, respectively. For $Re_p \ll 1$, creeping flow regime, the viscous effect dominates over the inertia and the drag

coefficient can be expressed by using Stokes' law, $C_D = 24/Re_p$. On the contrary, for Re_p in the range of 700 to 10^5, the inertia effect is predominant and Newton's relation, $C_D \cong 0.44$, covers the range [39], [40]. Moreover, if a particle is in a uniform bed of particles having bed voidage, ε, the drag force on a single particle in the bed is $\varepsilon^{-3.8}$ times that on a single isolated particle, leading to the following correlation for the drag force on a particle in a particle bed for both the Stokes' and Netwton's law regions [40]:

$$F_{d\varepsilon} = C_D \frac{\pi {d_p}^2}{4} \frac{\rho_f {u_0}^2}{2} \varepsilon^{-3.8} \quad (3)$$

II.2. Buoyant Weight

When the bed is fluidized, it exhibits fluid-like behavior and the density of the fluidized bed ρ_{fb} is:

$$\rho_{fb} = \varepsilon\rho_f + (1-\varepsilon)\rho_p \quad (4)$$

where ρ_p is particle density. The buoyancy force F_b on a spherical particle is defined as [7]:

$$F_b = \frac{\pi {d_p}^3}{6} \rho_a g = \frac{\pi {d_p}^3}{6} \varepsilon\rho_f + (1-\varepsilon)\rho_p g \quad (5)$$

where g is the gravity field. Accordingly, the buoyant weight W_b of the particle is:

$$W_b = gravity\ force - buoyancy\ force = \frac{\pi {d_p}^3}{6} (\rho_p - \rho_f) g\varepsilon \quad (6)$$

II.3. Interparticle Forces

Cohesion between particles may originate from a variety of sources. Van der Waals force, electrostatic force, and capillary force are considered as the main forces in particle adhesion [41]. These forces significantly affect the fluidization behavior of group A and, in particular group, C powders [13].

II.3.1. Van der Waals Force

Van der Waals was the first to point out that the nonideality of gases can be explained by the existence of molecular interactions due to interacting dipoles. The dispersion effect, which is the interaction between the instantaneous dipoles formed in the atoms by their orbiting electrons, is responsible for van der Waals force [42]. The very rapidly changing dipole of one atom generates an electric field that impacts the polarizability of a neighboring atom. The induced dipole of the neighboring atom tends to move in phase with the original dipole, producing a generalized attractive interaction known as the van der Waals force. This kind of force exists not only between individual atoms and molecules, but also between macroscopic solids. According to Krupp [43], Molerus [44] and Massimilla and Donsi [45], the van der Waals force between two smooth spheres of radius R at a separation distance Z, is given by:

$$F_{vdw} = \frac{h\bar{\omega}}{8\pi Z^2} R \left(1 + \frac{h\bar{\omega}}{8\pi^2 Z^3 H_r}\right) \quad (7)$$

where $h\bar{\omega}$ is the Liftshits-van der Waals coefficient and a function of the nature of the bodies in contact and of the surrounding medium and H_r is the hardness of the softer of two bodies. Krupp [43] suggested a value of 4 A^o for Z, the distance where van der Waals force is maxima and a value of $10^8\ N/m^2$ for the hardness of undeformable solids. In the case of contact between two spherical particles of different radii, R_1 and R_2, van der Waals force can be calculated from Eq. (7) assuming:

$$R = \frac{R_1 R_2}{R_1 + R_2} \quad (8)$$

Most powders have a rough surface with many asperities [46]. As a result of these asperities observed with real materials, a characterizing surface geometry and not the size of particles in contact should be considered. According to Krupp [43] and Massimilla and Donsi [45], a typical value of 0.1 μm can be considered for asperity size R_{as} and should be inserted in Eq. (8).

Although the relative significance of a particular form of interparticle forces strongly depends on the original properties of particles, the fluidized bed set-up and the fluidizing conditions, like moisture content [47], it is generally believed that the van der Waals force is much more significant than other types of interparticle forces for fine particles of a diameter less than 100 μm in a dry gaseous environment [13]. In addition, this force dominates over gravitational force and, hence, over fluid-dynamic forces generated in a fluidized bed under this condition [13], [48], [49]. The situation changes when porous particles or particles having a partly flattened surface, due either to their inherent structure, e.g., crystalline material, or to plastic deformation induced by pressure or an increase in temperature, are considered. For these cases, the region is extended to even larger particles [13].

II.3.2. Electrostatic Force

In addition to van der Waals force, electrostatic force can also contribute to the adhesion of particles and, hence, their aggregation in a gaseous environment [13], [43]. During the processing of powders under dry conditions, when non-conducting particles come into contact with surfaces of dissimilar material or slide along such surfaces, this is generally accompanied by an exchange of electrons in the surface layer. This causes

the particles to be electrically charged and the phenomenon is termed as a contact electrification or triboelectrification process [50], [51]. The motion of a charged particle in a gas-solid flow is influenced by the electrostatic force imposed on it by nearby charged particles. According to the well-known Coulomb's law, the electrostatic force between two charged objects, which are much smaller than the distance between them, is proportional to the product of the charges and inversely proportional to the square of the distance of separation [39]. This force is acting along a straight line from one charged object to the other and can be expressed by:

$$F_e = \frac{1}{4\pi\epsilon}\frac{q_1 q_2}{s^2} \quad (9)$$

where q_1 and q_2 are the charges carried by the two objects, s is the distance between the two objects, and ϵ is the permittivity of the surrounding medium.

In general, electrostatic force is insignificant compared to the first class of interparticle forces, van der Waals force [13], [51]. Moreover, this force vanishes in a humid environment due to a discharging of the system [13].

II.3.3. Capillary Force

Capillary force, liquid-bridge force, is caused by the condensation of moisture from the surrounding gas on the surface of particles, which then forms a liquid bridge in the gap between neighboring particles, as shown in Fig. 1. This produces a resultant attractive force between the two bodies as a result of the pressure deficiency in the bulk of the liquid and the surface tension of the liquid acting on the two particles [13], [51], [52]. The interparticle forces, which in a dry environment are principally due to van der Waals force, are then increased by this force [13]. Capillary force can dominate the gravitational force on the individual particles when the vapour pressure of the surrounding gas is close to the saturation pressure and can also be rather larger than the maximum van der Waals force as well [49], [51]. It is practically important in agglomeration processes, driers, and some kinds of reactors and bioreactors, as for example, in drying solids where it may severely hinder the handling of powders, especially at the start [49], [51]. The liquid-bridge force is the sum of the surface tension F_γ and the pressure differential across the air-liquid interface F_p [49], [53].

By approximating the bridge profile as circular arc (torus), capillary force can be estimated according to two methods, which differ in the place where forces act [53]. The first method is the boundary method, where the total force between two equal radii of R is calculated at the liquid-solid contact, considering F_p acting at the axially projected area of the liquid contact on the sphere and F_γ acting on the three phase contact line [52].

By this method, the total force can be defined as the following:

$$F_c = 2\pi\gamma R\, sin\alpha \sin(\alpha+\beta) + \pi R^2\, \Delta p\, sin^2\alpha \quad (10)$$

where γ is the liquid surface tension, α is the half-filling angle, and β is the contact angle. The differential pressure Δp across the air-liquid interface is given by the Laplace-Young equation, which can be expressed by:

$$\Delta p = \gamma\left(\frac{1}{r_1} - \frac{1}{r_2}\right) \quad (11)$$

where r_1 and r_2 are the liquid bridge meridional curvature radius and the liquid bridge neck radius, respectively [52], [53]. The magnitude of the total force is difficult to be precisely computed by this method, even for spheres [49].

However, the second method, the gorge method, in which the total capillary force is calculated at the neck of the bridge, enables a simple and sufficiently accurate result to be obtained [49], [53]. On the basis of this method, the total force can be approximated by:

$$F_c = 2\pi\gamma R \quad (12)$$

According to Massimilla and Donsi [45], similar to van der Waals force, surface asperities need to be taken into account in Eq. (12) to have reliable value for the capillary force.

It is worth mentioning that in most powder operations, vapour pressure is so low that the capillary force can be neglected [51].

A schematic comparison of different kinds of interparticle forces with that of the particle weight was provided by Seville et al. [49], as shown in Fig. 2, for a sample particle with a particle density equal to 3×10^{-3} kg/m^3.

In this figure, magnitudes of both capillary and van der Waals forces are calculated using actual particle radius and particle asperity radius, $R_{as} = 0.1\,\mu m$. Results of these calculations are plotted in the form of solid and dashed lines, respectively.

It can be seen that if the gross particle radius is taken into account, a particle diameter in the order of 1 mm exhibits interparticle van der Waals force approximately equal to the particle weight, which is less plausible.

On the contrary, when the latter radius is used, the equality of van der Waals force and particle weight is achieved for a $100\,\mu m$ particle size for which adhering to surfaces and resisting the force of gravity is commonly observed [49].

Also, it can be found from this figure that the magnitude of the liquid-bridge force, when present in the system, is greater than the maximum van der Waals force.

Moreover, it is clear that the ratio of interparticle cohesive force to gravity force increases by a reduction in particle size.

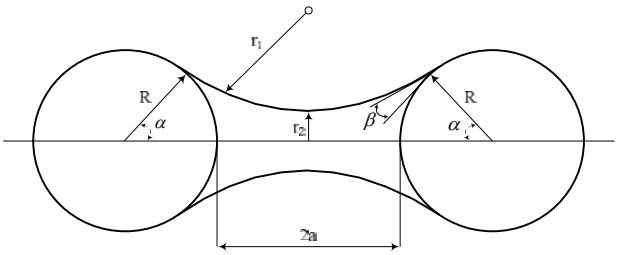

Fig. 1. Liquid bridge between two equal size spheres.
a = Half-particle distance

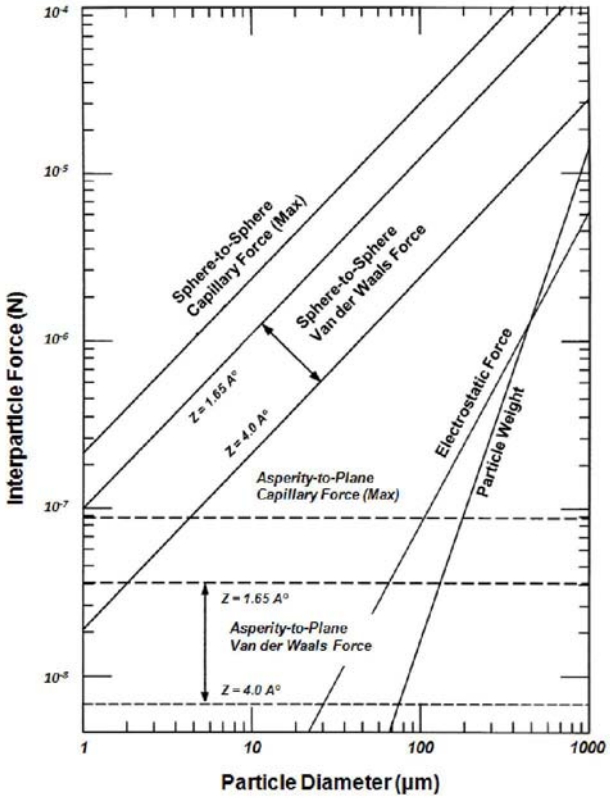

Fig. 2. Comparison of various interparticle cohesive forces with that of the particle weight. Adapted from [49]

III. Fluidization of Nanoparticles with High Interparticle Forces

According to Geldart's classification, for coarse particles of groups B and D, gravity force is always superior to interparticle forces and, hence, fluidization behavior is dominated by gravity effects. By reducing the particle size down to group A particles, the ratio of interparticle forces to the particle weight increases and these forces are of comparable magnitude for this group of materials [44]. Also, for small particles of this group, interparticle forces do not allow free fluidization in an increasing flow experiment until the drag force on the hindered bed is able to counteract the cohesion force, dislodge the particles, and restore a more normal fluidized stable state [15]. With a further decrease in particle size, entering group C region, cohesion between particles tends to predominate over the gravity force giving rise to substantial bulk adhesion that leads to significant reduction in the permeability of the particle assembly by the interstitial gas [54]. In the case of dry fine particles ($d_p < \sim 30\ \mu m$), the interparticle forces are dominant and may exceed the particle weight by several orders of magnitude [48], [49].

Under Geldart's classification, class C covers the range of particles having a mean diameter less than $20\ \mu m$ and denoting a density difference between gas and solids larger than 1000 kg/m^3. It has been found that due to strong interparticle forces normal fluidization of these powders is extremely difficult; unlike other classes, they cannot be fluidized individually, even up to terminal velocity of original particles, and the process of fluidizing them usually involves plugging, channeling, and the formation of stable cakes [10], [15], [44], [54]. However, this is not a generalized fluidization behavior of solid materials belonging to this group. On the basis of Geldart's classification, submicron and nanoparticles are at the extreme of group C particles suggesting at first sight that the fluidization would prove impossible due to the strong interparticle forces between solids [54]. Nonetheless, it has been experimentally found that at gas velocities far above the minimum fluidization of the primary particles, such very fine powders form dynamically stable agglomerate structures, made up of the constitutive particles, in the bed and can then grow to sizes in the micron or millimeter ranges and whose fluidization behavior could therefore very well fall within groups A, B, and even C [12], [15]-[20], [55]. As these particles agglomerate into larger structures, the balance between the interparticle and inertial forces in the particulate system changes [21]. Consequently, the existence of these micro-structure agglomerates is the reason to prevent the formation of stable cohesive bonds between the primary particles and, hence, presenting a potential deviation from the theoretical behavior of cohesive materials observed in group C powders [54].

Therefore, the fine particles of group C powders can be classified into three main subclasses according to their fluidization behavior. The first subclass includes all particles that can never be fluidized under any circumstance because of extra strong adhesion forces between fine particles and between agglomerates [19], [20], [55]. For this type of particles, channeling and plugging always happens and there are two cases that show such behaviors. In one case, channels or rat-holes are directly formed from individual fine particles with a particle size in the range of several microns to tens of microns and there is a lack of adhesion forces between these powders to cause agglomeration. In the other case, channels or plugs are formed by the agglomerates of fine particles with a particle size smaller than $1\ \mu m$ and showing appreciable adhesion between agglomerates. Experiments show that the use of external forces, like vibration, can help to break these channels and plugs to obtain stable fluidization [55]. The second and third subclasses are comprised of powders that can cross the

fluidizability barrier by forming agglomerates of primary particles. However, these subclasses have some differences in their natures and are defined as agglomerate particulate fluidization (APF) and agglomerate bubbling fluidization (ABF). These behaviors can be usually found in the case of submicron and nanoparticles as well as some cases of micron size fine particles. More explanations concerning the last two subclasses are provided in the following section.

III.1. Agglomerate Fluidization

III.1.1. Agglomerate Particulate Fluidization and Agglomerate Bubbling Fluidization

Agglomerate fluidization is a common mode of fluidization for ultrafine particles [19]. Chaouki et al. [15] first found that at superficial gas velocities in excess of 0.04 m/s, which were far above the minimum fluidization of the original particles, the aerogel particles rearranged themselves into clusters and then these new entities fluidized uniformly and homogeneously. The agglomeration of original ultrafine particles at gas velocities much larger than incipient buoyancy conditions of the primary particles have been reported by other researchers [12], [16]-[20], [55], especially for nano size particles.

This is more plausible due to the fact that cohesive forces between nanoparticles significantly increase with decreasing particle size, thus nano size powders coalesce easier than micron-size particles [20]. Accordingly, gas fluidization of nanoparticles refers to fluidization of nanoparticle agglomerates [1]. In this regard, the fluidization behavior of agglomerates can be classified as agglomerate particulate fluidization (APF) and agglomerate bubbling fluidization (ABF).

Usually, powder systems with a very small primary particle size, nanosize, and a very low bulk density can achieve APF behavior. Figs. 3 show the sketch of the fluidization behavior of APF particles. At very low gas velocities, preferential channeling generally happens in the bed, as exhibited in Fig. 3(a), but upon increasing the superficial gas velocity, since the channels are so weak, the particles beside the channels or at the top of the bed start to fluidize first, causing the channels to break and disappear.

Then the fluidized region continuously expands until the whole bed reorganizes itself into a new uniformly fluidizing state and agglomerate fluidization is thus set into action. During fluidization, neither a dead region, nor bubbles can be found [19], [20].

Stable agglomerates, which form from the constitutive nano size particles, have snowflake like configurations and smoothly fluidize at velocities much larger than the expected minimum fluidization velocity of primary particles. The agglomerates are very light and, hence, can be easily moved with gas, even in the turbulent gas wave. By increasing the agglomerates' size, they will have high terminal velocity.

For gas velocities lower than the terminal velocity of the agglomerates, they will fall back and remain in the bed.

Therefore, the uniform fluidized bed has a clear solid surface in a large window of gas velocities, as shown in Fig. 3(b). A high degree of mixing is the main consequence of such freely flowing behavior that is advantageous for heat and mass transfer efficiency in the bed compared to a fixed or a bubbling fluidized bed. At higher gas velocities, the fluidized bed smoothly expands and the bed surface becomes unclear due to the entrainment of small agglomerates, as shown in Fig. 3(c). At even much higher gas velocities, pneumatic transport regime begins and masses of agglomerates are carried away and the bed will finally be empty [19], [20], as shown in Fig. 3(d).

Considering the agglomerates as fluidizing particles in the bed, the expanded bed has a texture, which is very similar to the particulate fluidization in a liquid-solid system than to the bubbling fluidization in a gas-solid system.

In this case, since agglomerates are so light, the density difference between agglomerates and the surrounding gas is very close to that of liquid-solid surrounding gas is very close to that of liquid-solid systems.

Therefore, nanoparticles having such homogeneous fluidization behavior are classified as agglomerate particulate fluidization, which is completely different from agglomerate bubbling fluidization [19], [20].

According to Chaouki et al. [15] and Wang et al. [19], the possibility of the occurrence of APF behavior is linked to the instability of jetting or channeling in the original fixed bed. In fact, the relative ease in dissipating channels certainly depends on the porosity of the fixed bed or in other words, on the particulate bed's bulk density. The possibility of this instability increases by decreasing the bulk density of the system and, hence, gives rise to the occurrence of agglomeration in the bed to be more feasible.

In the case of ABF, primary particles are larger (micron, submicron or nanosize) and have a higher bulk density compared with particles that show APF behavior. As a result, the particulate system is less able to easily break the channels and make the fluidizing mode a homogeneous one.

Moreover, this prevents transforming the whole bed into a new system with a new effective dynamic size and apparent weight in which the hydrodynamic forces govern the gas-agglomerate interaction. In this situation, because of the partly local dominance of cohesion over the inertial force, the bed behaves like a system in between the classical group C behavior and the homogeneous fluidized bed.

When these particles agglomerate during fluidization, winding channels are formed inside the bed, causing alternating fixed and fluidized regions, and accompanied by bubbling.

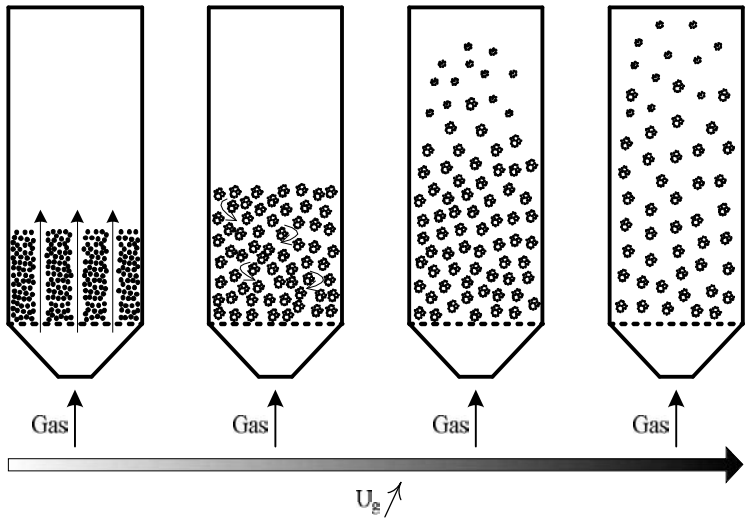

Fig. 3. Sketch of fluidization of APF particles. Adapted from [19]

Stratification phenomenon generally occurs for these agglomerates along the bed height, by the presence of a fixed bed or slow moving large agglomerates at the bottom, a fluidized region of smaller agglomerates in the middle and a dilute-phase region of even smaller agglomerates, including individual particles, further up in the fluidized bed [55], as depicted in Fig. 4.

Lowering the size and bulk density of primary particles are factors that can assist a bed with ABF behavior to become more similar to APF behavior.

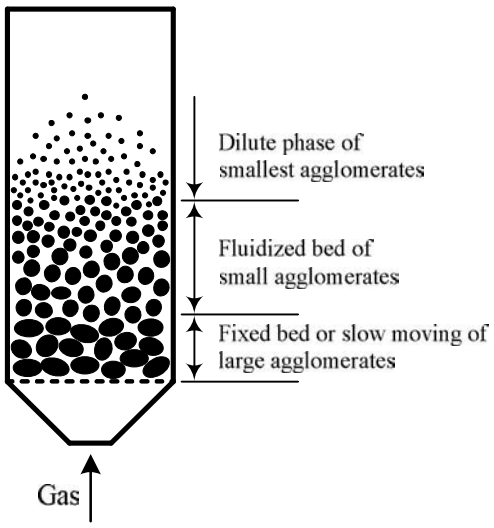

Fig. 4. Stratification phenomenon in ABF agglomerate fluidized bed. Adapted from [55]

Considering the above-mentioned philosophy, APF agglomerates are characterized by smooth/particulate fluidization with a low minimum fluidization velocity, negligible elutriation of particles, very large bed expansion (up to five times the initial bed height), a well defined gas-solid interface and minimal bubbling even at high superficial gas velocities. These agglomerates also have narrow agglomerate size distribution, which uniformly distribute throughout the bed. In contrast, ABF agglomerates have difficulties at low superficial gas velocities to be fluidized and show channels, slugs and spouting. Moreover, they exhibit low bed expansion (less than two times the initial bed height), high minimum fluidization velocity, large bubbles, considerable elutriation of particles, a poorly defined gas-solid interface and non-uniform distribution of agglomerates in the bed where the smaller ones appear to be fluidized in the upper part and the larger ones slowly move or are defluidized at the bottom of the bed [1], [9], [20], [22].

A summary of notable differences between ABF and APF agglomerates and their fluidization behaviors is presented in Table I.

TABLE I
COMPARISON OF THE FLUIDIZATION BEHAVIOR OF APF AND ABF [19], [20], [22]

	APF	ABF
Primary particle size	Nanoparticles	Micro, Submicron, Nanoparticles
Agglomerates	Loose, multi-stage, light in weight	Dense, single-stage, heavy in weight
Bulk density	Low (< 100 kg/m^3)	High (> 100 kg/m^3)
Fluidization characteristics	1. Low minimum fluidization velocity 2. Bubbleless 3. Bed expansion ratio is high 4. Agglomerates are uniformly distributed in the bed 5. Fluidized bed homogeneously expands, and the bed density decreases with increasing gas velocity 6. Negligible elutriation	1. High minimum fluidization velocity 2. With bubbles 3. Bed expansion ratio is low 4. Large agglomerates are at the bottom of the bed, with small ones at the top 5. Bed expansion ratio and emulsion phase density do not change much with increasing gas velocity 6. Considerable elutriation

III.1.2. Agglomerate Structure

The famous Geldart classification diagram predicts the

fluidization behavior of powders based on the size of a single particle and the density difference between solids and fluid [49].

Although this classification has been of great value in facilitating the prediction of fluidization behavior for various particles, it suffers from some deficiencies.

As for example, when some fluidization operating parameters (pressure, temperature, gas properties, and effective gravitational acceleration) change, the hydrodynamic/interparticle force balance may change, this could result in a change in demarcation of particle groups [56]. Also, this simple classification cannot predict the transition from group B powders to A and even C as a result of inducing external interparticle forces to the particulate system reported by Seville and Clift [57], Rhodes et al. [58], and Shabanian et al. [59]. This deficiency can be compensated by the addition of a third axis corresponding to the magnitude of external interparticle forces into the original two dimensional Geldart's diagram.

Furthermore, as pointed out in the case of agglomerate fluidization, the physical properties of primary particles cannot properly measure to predict their fluidization behavior [17], [20]. Instead, the hydrodynamic behavior of agglomerate fluidization is closely related to the properties of the agglomerates, including their size, density, structure, etc [19], [20]. In addition, various factors, such as capillary and electrostatic attraction, geometry, and adsorption, influence the particle agglomeration process and, therefore, their fluidization. Among all these factors, agglomerate structure has vital importance for agglomerate fluidization of ultrafine powders [20].

Fluidization behavior of APF particles is quite different from normal group C powders and can be smoothly fluidized in a gas-solid particulate fluidization regime with a high bed expansion ratio and bubbleless behavior via micro-structure self agglomeration [20]. In fact, the main conditions to achieve such behavior for some nanoparticles are to have, first, a particulate system with very low bulk density and, next, fluidizing entities that are large enough for hydrodynamic forces to merely control the fluidization behavior and have strong adhesion forces in their own structures to withstand gas drag force [19]. It is rational to believe that low bulk density causes a loose agglomerate structure of bonded nanoparticles, which are strong enough to hold large amounts of gas [20].

Yao et al. [20] studied the fluidization properties of APF particles and stated that unique fluidization behavior of these powders is due to a multistage agglomerate (MSA) structure. At first, primary nanoparticles tend to arrange in a three dimensional chain-like structure, as shown in Fig. 5, that can grow up to several hundred nanometers. These particles can be bonded together in two paths.

In one path, the chain-like structure can be formed via coagulation of aerosol particles during the manufacturing process of nanoparticles. These bonds are very firm and are identified by sintered areas at the contact points between primary nanopowders.

In the other way, chains form from the effect of the strong van der Waals force on such tiny particles. Chains resulting from the latter are not rigid enough and can be broken apart during fluidization, but will reform via dynamic agglomeration [21]. Overall, this three dimensional structure is the main reason for having low bulk density of these powders. Second, the three dimensional chain-like structures coalesce into larger agglomerates most of which are $1-100\ \mu m$ and named as simple agglomerates.

Finally, many small simple agglomerates joined together and formed large agglomerates when fluidized. These large fluidized agglomerates were defined as complex agglomerates.

Complex agglomerates show dynamic behavior during fluidization by continuous breaking and reforming. This dynamic process is actually a balance between the separation and the congregation of simple agglomerates. Therefore, the fluidization process of APF particles can be considered as a self-rearranging process of simple agglomerates. This process finally reaches an equilibrium point at which a stable complex agglomerate size is achieved [20].

In brief, MSA structure is an important feature in the fluidization of ultrafine powders. Particles that show APF behaviors create a very porous structure in the bed due to the formation of many porous three dimensional chain-like structures and, hence, the strong adhesion forces between tiny particles are effectively diminished and the packed bed does not become compacted. Therefore, simple agglomerates are very light and have limited connecting points between each other, which allows the packed bed to be easily broken and fluidized, when gases pass through the channels [20].

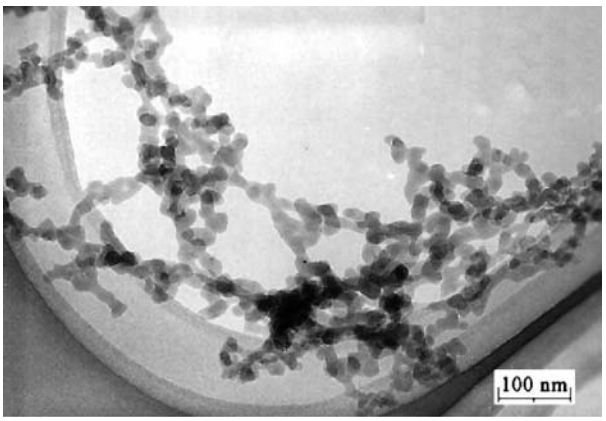

Fig. 5. Transmission electron micrograph (TEM) of Aerosil 300, $dp = 7nm,\ \rho_b = 37.15\ kg/m^3$. Adapted from [20]

However, Yao et al. [20] stated that ABF particles, unlike APF ones, possess a single-stage agglomerate (SSA) structure. Fine particles of this subclass tend to form drop-like agglomerates, such as simple agglomerates, whenever relative motion exists between

particles, during packaging, handling, shipping, and storage.

Generally, simple agglomerates of large size ABF particles are comprised of pile up structures, which are very unstable [55] compared to those of APF ones because of less cohesion forces that exist between the member particles. The presence of these structures rather than chain-like, which is responsible for having low bulk density in the particulate system, results in a compact nature for the packed bed.

As a consequence, difficulties arise for the disintegration of channels in these beds. By decreasing the original particle size, a chain-like structure begins to form, which not only increases the porosity of the agglomerate but also enhances their stability.

Similar to complex agglomerates of APF particles, when simple agglomerates of ABF powders are fluidized, they contribute to the dynamic process and their size and shape undergo successive changes. During fluidization, these simple agglomerates experience rearrangement with respect to their constitutive particles, or are broken apart into smaller agglomerates or even individual particles [55].

III.1.3. Simple Classification Criteria to Discriminate Between APF and ABF

Geldart et al. [60] presented an empirical classification criterion to predict the fluidization behavior of cohesive powders based on the so-called Hausner ratio, which is the ratio of the aerated ρ_b to tapped ρ_{tb} bulk density of the powder.

According to this criterion, cohesive powders, which are difficult to fluidize, produce high Hausner ratios. It was found that powders having a ratio less than 1.25 appear to be fluidized like group A, while the fluidization behavior for powders with a ratio higher than 1.4 is clearly similar to the classical behavior of group C. For powders with the Hausner ratio between 1.25 and 1.4 they possess characteristics of both A and C groups. Although, this criterion provides appreciable results for micron size fine particles, Esmaeili et al. [9] found that it cannot satisfactorily predict the APF and ABF fluidization behaviors of nano size particles.

It is believed that the bulk density of the particulate system has a crucial effect on the APF or ABF fluidization behavior of tiny particles [1], [15], [19], [20].

In this regard, according to their experimental results, Yao et al. [20] and Zhu et al. [1] reported that relatively small (<20 nm) nanoparticles with a bulk density less than 100 kg/m^3 are characterized as APF, while those with a larger size and higher bulk densities appear to behave as ABF. This criterion has been tested by many researchers and, fortunately, nearly all of them reported acceptable results with it.

In addition, Zhu et al. [1] showed that the classification criterion proposed by Romero and Johanson [61] for differentiating between homogeneous and bubbling fluidization of classical fluidized particles based on the value of a combination of dimensionless groups can substantially keep its predictive ability to distinguish whether agglomerates behave as APF or ABF. According to this classification, a bed can be smoothly fluidized if the product Π value of the combination of dimensionless groups, including the particle to fluid density ratio, the Reynolds and Froude numbers at the minimum fluidization velocity, Re_{mf}, Fr_{mf}, and the bed height at the minimum fluidization velocity H_{mf} to column diameter D_{col} ratio, is less than 100, whereas the one with a higher product value appears to have bubbling fluidization behavior:

$$\Pi = Re_{mf}\, Fr_{mf}\, \frac{\rho_p - \rho_f}{\rho_f}\, \frac{H_{mf}}{D_{col}} < 100 \text{ smooth fluidization,}$$

$$\Pi = Re_{mf}\, Fr_{mf}\, \frac{\rho_p - \rho_f}{\rho_f}\, \frac{H_{mf}}{D_{col}} > 100 \text{ bubbling fluidization.}$$

Results of Zhu et al. [1] show that this criterion has very high sensitivity and is superior to simply exploiting the size and bulk density of powders to differentiate between APF and ABF behaviors of agglomerates.

Table II exhibits the comparison of Romero and Johanson's criterion to that of Yao et al. [20] and Zhu et al. [1] for some ultrafine particles.

TABLE II
COMPARISON OF THE PREDICTIVE ABILITY OF ROMERO AND JOHANSON'S CRITERION TO THAT OF YAO ET AL. [20] AND ZHU ET AL. [1] TO DISTINGUISH THE APF AND ABF FLUIDIZATION BEHAVIOR OF ULTRAFINE PARTICLES. ADAPTED FROM [1]

Powder		Particle primary size	Particle bulk density	Π	Fluidization type
Trade no.	Material	(nm)	(kg/m^3)		
R974	SiO_2 Hydrophobic	12	33.24	0.008	APF
R104	SiO_2 Hydrophobic	12	62.90	0.197	APF
R106	SiO_2 Hydrophobic	7	41.49	0.008	APF
R972	SiO_2 Hydrophobic	16	39.00	0.010	APF
A300	SiO_2 Hydrophilic	7	39.00	1.19	APF
OX50	SiO_2 Hydrophilic	40	121.33	398	ABF
	TiO_2 Hydrophilic	21	128.29	927	ABF

It can be found from the table that for APF nanoparticles, the Π value is much less than 100, while for ABF nanoparticles, it is much higher than 100, which, in fact, shows the appreciable evel of certainty of applying this criterion.

Although the Romero and Johanson's criterion presents spectacular ability for the prediction of APF and ABF fluidization behavior of ultrafine powders, it was only verified for some nanoparticles [1], and more research is required to confirm this classification

criterion is indeed applicable for all nanoparticles.

IV. Assisting Methods

As discussed, the cohesive fine particles and nanopowders can be fluidized at superficial gas velocities greatly exceeding the minimum fluidization velocity of the primary particles in the form of agglomerates even without any assisting methods [62].

However, for the conventional gravity-driven fluidization of ultrafine particles, even in particulate fluidization, appreciable powder elutriation happens at the high superficial gas velocities required to fluidize the agglomerates.

This loss of particles is probably the main reason that prevents the application of gas fluidization of fine particle agglomerates, especially nano-agglomerates, in industrial processes [1], [23], [63].

Moreover, although agglomeration makes it possible to fluidize ultrafine particles, it limits their potential because of the undesired decrease in specific surface area and increase in heat and mass resistances [11], [25], [34]. Therefore, it is preferable to improve the fluidization quality of these powders to work at lower gas velocities, have smaller agglomerates, and more homogeneous gas-solid flow to properly exploit their potential.

To this aim, various assisting methods have been developed. They include acoustic wave, mechanical vibration, magnetic/electric fields, the use of a centrifugal fluidized bed and a tapered fluidized bed, the addition of foreign particles, and the use of micro-jets as a secondary flow in the bed.

The degree of fluidization enhancement achieved by applying these methods is evaluated by measuring some hydrodynamic parameters, such as the minimum fluidization velocity, bed pressure drop, bed expansion, agglomerate size, degree of mixing, bubble suppression and amount of powder elutriation, as indicators of fluidization quality.

In this brief, these methods and their impacts on fluidization quality will be discussed.

IV.1. Sound Assisted Fluidization

Various researchers have studied the phenomenology of beds of cohesive powders fluidized under the influence of acoustic fields of various sound pressure levels and frequencies.

For the first time, by using an acoustic field generated by loudspeakers located at the bottom of the bed, Morse [64] found that fluidization of micron size particles under conditions where they possessed intense channeling or slugging was achieved provided an acoustic field with a frequency f_S in the range of 50 and 500 Hz, and a sound pressure level (SPL) larger than 100 dB.

Chirone et al. [65], [66] reported that the application of sound waves at a specific frequency, 120 Hz, and SPL in the range of 100–150, resulted in bubble free fluidization typical of group A powders in beds of cohesive particles of $1-45\ \mu m$ in size, as a consequence of the disaggregation of large agglomerates into smaller ones. In addition, it was noted that the high intensity sound could substantially reduce the entrainment of fine particles [65].

Extending their work, Russo et al. [67] showed that for beds of micron and submicron size particles, at a given SPL, fluidization behavior could only be improved within a certain range of sound frequencies (between 110 and 140 Hz) above/below which channeling occurred. The combined effects of gas velocity, sound frequency and pressure level on bubbling behavior were investigated by Levy et al. [68].

They found that at the natural frequency of the bed of micron size adhesive particles, high intensity sound waves caused reductions in both the minimum fluidization and minimum bubbling velocities.

Also, an increase in SPL led to a decrease in bed expansion and an increase in bubble frequency. With the aid of an acoustic field having a low frequency and a high sound pressure level, Guo et al. [69] obtained a homogeneously fluidized bed for micron size fine powders.

Experimental studies to scrutinize the effect of sound wave excitation on particulate beds of nanoparticle agglomerates was started in 2004 by Zhu and coworkers [23].

It was demonstrated that for SiO_2 nanoparticles with a primary particle size of 12 nm, channeling or slugging of the bed disappeared, minimum fluidization velocity was substantially reduced, and elutriation of nanoparticle agglomerates was to a large extent weakened at low frequency.

By increasing the sound frequency, in the range of 200 – 600 Hz, bubbling fluidization occurred.

Also, a minimum level of sound pressure, 115 dB, was required for sound waves to impact the fluidization behavior of nano-agglomerates [23].

Guo et al. [63], [70], [71] and Liu et al. [24] in a series of works showed that for particles in the range of micron, submicron, and nano size, smooth fluidization could be achieved with the help of an acoustic field at low frequencies due to disrupting large agglomerates. It was also noted that at a fixed sound pressure level, minimum fluidization of powders was reduced by increasing the sound frequency up to a critical value, while the reverse occurred at higher frequencies.

A similar trend was observed for the agglomerate size under the effect of sound agitation for nano size particles [71].

In addition, it was found that at the same sound frequency, the quality of fluidization was significantly enhanced (agglomerate size and minimum fluidization decreased) with an increasing sound pressure level in the range of 100 – 103.4 [24], [69], [71]. Ammendola et al. [11], [25] characterized the fluidization behavior of two nanoparticles with APF and ABF behaviors under the application of acoustic fields of different SPLs and frequencies.

It was noticed that either for the case of increasing SPL at a constant frequency or operating at an optimum frequency range and constant SPL, minimum fluidization velocity and agglomerate size decreased and bed pressure drop and bed expansion increased.

Similar to Zhu et al. [23], they indicated that minimum SPL (SPL_{min}) was required to obtain good fluidization quality for both powders, while the SPL_{min} for APF nanoparticles was lower than for ABF ones. In addition, it was observed that the mixing of these nanopowders was intensified under the influence of sound waves from a completely segregated state in a non-assisted fluidized bed. Under the best conditions, mixing could be achieved up to microscale but not in smaller scales.

A similar result was reported by Ammendola and Chirone [26] for blending two ABF nanoparticles when the bed was assisted by sound agitations.

Unlike other works in the case of nano-agglomerates, Kaliyaperumal et al. [27] used a sound source under the distributor plate to study the effect of sound vibration on the fluidization behavior of nano and submicron particles. They found that acoustic waves brought about a decrease in minimum fluidization velocity and an increase in bed pressure drop and bed expansion for both kinds of particles.

Similar to other studies, there was an optimum range for sound frequency and SPL_{min} was 110 dB, below which the impact of acoustic waves was insignificant.

Furthermore, they observed that the best result for fluidization quality was obtained at a sound frequency close to the natural frequency of the bed.

Among the studies for enhancing the fluidization quality of fine/ultrafine powders by an acoustic field, Morse [64] and Kaliyaperumal et al. [27] positioned the sound source below the bed, while others located the source in the freeboard.

Although Kaliyaperumal et al. [27] claimed that introducing acoustic waves from the bottom of the bed can lead to a more uniform agglomeration size due to absorbing more sound waves by larger agglomerates at the bottom of the bed and increasing the possibility of their disintegration, an appreciable difference between these two cases based on measurements of general fluidization parameters, such as minimum fluidization velocity, bed pressure drop, bed expansion, range of optimum sound frequency, etc, was not observed.

In this regard, having a more comprehensive study, including the measurement of agglomerate size along the bed height, is required to determine whether introducing sound waves below the distributor can result in a more uniform agglomeration size in the bed or not.

There are three main issues that nearly all researchers have pointed out for sound assisted fluidization of fine/ultrafine powders.

First, there is a minimum sound pressure level below which the acoustic field does not have any effect on the fluidization quality of fine powders. It can be explained as follows: since the acoustic oscillation strength is proportional to the sound pressure level [27], a minimum sound strength, or energy, is needed to initiate the fluidization or improve the fluidization quality. Secondly, by increasing the sound pressure level, since the energy given to the bed increases, the quality of the fluidization becomes better.

However, at very high SPL, this might be reversed due to a higher possibility of collision between particles and agglomerates, which causes a large agglomerate size [71].

Lastly, the effect of sound frequency on fluidization quality is not monotonic and an optimum range or value has been determined for different powders most of which were close to the natural frequency of the particulate bed. The explanation of this trend is not straightforward; for low frequencies, the relative motion between smaller and larger agglomerates is practically absent and, hence, there is no break-up of agglomerates [11], [26].

In other words, a period of acoustic excitation is long with respect to the time needed for the flow of fluidizing gas to set up local channeling in the bed, which, after the initial perturbation, has recovered its adhesion [67]. For high frequencies, the sound waves are not able to propagate inside the bed [11], [26].

In fact, the sound absorption coefficient is proportional to the square of sound frequency as sound propagates through the particulate bed.

Consequently, for high sound frequencies, most of the acoustic wave energy is absorbed by the upper part of the bed, if the sound source is located at the top, and reducing sound energy at the bed bottom fails to disrupt large agglomerates at the bottom of the bed and, hence, fluidization quality decreases [71]. If the source is located at the bottom of the bed, more sound energy would be absorbed by large agglomerates at the bottom and particles at the top of the bed would experience less excitation, which has a negative effect on the fluidization quality [27].

IV.2. Vibro-Fluidization

Similar to sound assisted fluidization, a considerable number of studies have been devoted to vibro-fluidization of fine/ultrafine particles. Cohesive micron and submicron powders have been successfully fluidized with the aid of mechanical vibration.

Employing a vibro-fluidized bed, Mori et al. [72] found that a wide range of fine particles down to the submicron level could be fluidized at relatively low gas velocities.

According to fluidizability of fine powders under the effect of vertical agitation, they classified group C fine particles into three subgroups: easily fluidized with large bed expansion; fluidizing powders under bubbling conditions with controllable entrainment; and non-fluidized powders even using the vibro-fluidized bed. Dutta and Dullea [14] used an external vibration and observed that the fluidization quality of micron size fine particles improved by a simultaneous increase in bed

pressure drop and bed expansion accompanied by a decrease in elutriation loss.

Marring et al. [73] and Noda et al. [74] reported that fluidization of cohesive powders was achieved when the bed was assisted by mechanical vibration.

Through in situ agglomerate size measurement using a pulsed laser coupled with a CCD camera, Wank et al. [75] obtained that the agglomerate size of Boron Nitride powders, $5-11\ \mu m$, decreased by increasing the force applied to the system due to vibration.

Mawatari et al. [76] stated that increasing the vibration intensity, which is defined as vibrational acceleration to gravitational acceleration, $\Gamma = A_m \frac{(2\pi f_V)}{g}$, where the A_m is the amplitude of vibration and f_V is the frequency of vibration, for group C micron size powders led to a decrease in minimum fluidization velocity and the elimination of channels and cracks, while the bed pressure drop remained fairly constant for different vibration intensities.

Comprehensive studies on the fluidization of fine particles under the application of vertical vibration were carried out by Xu et al. [77] and Xu and Zhu [47]. For a variety of micron and submicron solids, employing vibration reduced both the agglomerate size and the degree of stratification of agglomerates throughout the whole bed.

Unlike Wank et al. [75], they found that agglomerate size decreased with vibration intensity up to a critical value above which the reverse trend happened.

Somewhat similar results to those of Xu and Zhu [47] were reported by Valverde and Castellanos [78]. They noted that during fluidization of micron size cohesive powders assisted by vertical vibration, the homogeneous fluidization regime enlarged by increasing the vibration intensity to a critical value.

With further increase, visible bubbles were developed in the bed with a similar physical mechanism for bubble formation to non-vibrated fluidized beds.

Accordingly, they concluded that although vibration can reduce particle agglomeration to have APF behavior for a particulate bed of adhesive particles, agglomeration at some minimum level is required for APF behavior.

Nam et al. [32] performed the first study concerning the effect of vibration on the fluidization quality of nanoparticle agglomerates. They observed that silica nanopowders could be smoothly fluidized in the form of stable, very porous agglomerates with insignificant elutriation in the range of vibration frequency between 30–200 Hz.

It was shown that vibro-agitation was only initially required to disrupt interparticle networks in the particulate system after which aeration was sufficient to sustain the bed in a fluidized and expanded state for a long period of time.

A similar result was reported by Zhang and Zhao [79] employing a horizontal vibration system for a nanoparticle fluidized bed.

Nam et al. [32] also found that albeit a vibro-fluidized bed could significantly improve the fluidization quality of nanoparticles, processing the received materials by mechanical vibration was not feasible and large/hard agglomerates that existed in such powders sank to the bottom of the bed and did not break at all.

Moreover, their experimental results revealed only a weak effect of vibrational parameters on the bed pressure drop and minimum fluidization velocity.

Furthermore, the authors showed that nanofluidization assisted by external vibration could quickly mix nanopowders up to microscale. It was demonstrated by Hakim et al. [21] that decreasing interparticle (capillary and electrostatic) forces enhanced the fluidization quality of nanoparticles via decreasing the minimum fluidization velocity and agglomerate size. Similar results were observed when the nanoparticulate bed was subjected to mechanical vibration.

By exploiting the same experimental set-up, which was used by Nam et al. [32], Harris [80] could enhance the fluidization quality of APF nanopowders at relatively low frequencies, 16–34 Hz.

For different nanomaterials Yang et al. [33] found that at certain vibration amplitudes, by increasing the vibration frequency, which was equal to an increase in vibration intensity, the minimum fluidization velocity decreased and bed pressure drop and bed expansion increased.

They also showed that by employing the vibration excitation the n exponent in the Richardson-Zaki equation [81], which is an index of the degree of particulate fluidization for cohesive particles, increased by increasing the vibration frequency.

Wang et al. [82] reported that for a bed of SiO_2 nanoparticles under the influence of vibration, there was a critical vibration frequency corresponding to a minimum agglomerate size.

Most recently, Kaliyaperumal et al. [83] investigated the fluidization behavior of nano and submicron materials in a mechanically vibrated fluidized bed and found that the fluidization qualities of both powders were enhanced under those conditions.

Although all researchers believed that employing vibro-fluidized beds enhanced the fluidization quality of fine/ultrafine particles of group C powders, complete consensus regarding the effect of vibration on all fluidization parameters has not been achieved yet. For example, some authors reported that pressure drop increased as the vibration intensity increased [33], [82], [84], [85], some did not observe any change [32, 76], and some found that it decreased with vibration intensity [86].

Concerning the minimum fluidization velocity, Nam et al. [32] did not observe appreciable variation by vibration intensity, while some others found that it decreased as the vibration intensity increased [74], [76], [84], [86].

Moreover, there is no clear agreement on the effect of vibration strength on agglomerate size.

Wank et al. [75] reported that the agglomerate size decreased up to $\Gamma = 5.5$, while Xu and Zhu [47] and

Wang et al. [82] found there was a critical value of vibration intensity or frequency, much smaller than $\Gamma = 5.5$, above that agglomerate size increased rather than decreased.

Therefore, though there is no doubt that vibro-fluidization is one of the useful assisting techniques for improving the fluidization quality of fine/ultrafine particles, a more comprehensive study of this method is required to clarify the exact influence of vibrational parameters, namely vibration amplitude and frequency, on the fluidization behavior of these powders.

IV.3. Magnetically Assisted Fluidization

The application of an oscillating magnetic field is another beneficial assisting method to enhance the fluidization of fine/ultrafine particles. This technique has been generally implemented via the fluidization of either magnetic particles or a mixture of magnetic and nonmagnetic particles, under the exposure of an external magnetic field, which has been usually generated by a DC current [32], [87]-[91]. For the latter, both very fine and large magnetic particles have been used in experimental works.

Fine magnets often create chains along the field, while large ones, which have a larger size and/or density than those of fine bed materials, do not move along with fluidized particles and mainly remain close to the gas distributor.

Zhu and Li [88], [89] began employing this technique to improve the fluidization quality of group C powders. They studied the behavior of gas-solid fluidized beds with the mixture of ferro and non-ferro-magnetic powders both in the range of type C particles in an axial uniform magnetic field.

For the mixture material, the gas-solid fluidized bed was operating in agglomerate bubbling fluidization mode and, hence, they evaluated the impact of the magnetic field on the fluidization behavior through the measurement of bubble size. It was found that bubble size was highly dependent on magnetic field intensity, frequency, and the fraction of magnetic particles.

At a certain field frequency, bubble size decreased as field intensity increased.

Also, at a given magnetic field strength, bubble size increased by decreasing field frequency or fraction of magnets in the bed.

According to their experimental observations, they believed that the magnetic field could affect the fluidization of a fine particulate bed via the following mechanism: magnetic particles reorganized themselves to form a type of chain structure along magnetic field lines and this chain was the main reason for improving the fluidization quality for two reasons: first, the chain could easily penetrate the bubble from the top and break it due to a high ratio of gravitational force to drag force; second, the chain could restrain channeling. They noticed that the chain structures had two different actions to make the cohesive bed fluidized.

Those chain structures close to the channels tried to eliminate them and increase the resistance of gas passing through the channel when the right magnetic field intensity was applied and those chains that were in the particulate body tended to disintegrate the cake structure into smaller agglomerates leading to a decrease in the resistance of the gas passing through these agglomerates. In this way the completely defluidized bed was transformed into a fluidized bed with small bubbles by applying the optimum field intensity and frequency.

Similarly, Lu and Li [92] reported that the fluidization quality of the mixture of magnetic and non-magnetic cohesive type C particles was promoted with the help of a transverse rotating magnetic field.

They found that magnets displayed four kinds of motions in a rotating magnetic field, which included vibrating, forming rotating chains, moving around the walls, and keeping still.

As a result of these motions in the magnetic field, the channel could be eliminated, bubbles broken, and agglomerates disintegrated.

The first study to investigate the effect of an oscillating magnetic field on the fluidization of nanoparticle agglomerates was carried out by Yu et al. [30].

In their experiments large and heavy magnetic particles were used, which could not be fluidized by the action of gas drag force and remained rotating just above the gas distributor. They observed that the movement of magnetic particles, excited by an external magnetic field, greatly improved the fluidization of nanoagglomerates by disrupting large agglomerates, preventing the formation of bubbles, reducing the minimum fluidization velocity, and elutriation.

By using this technique they could easily and smoothly fluidize a mixture of soft (smaller than $500\ \mu m$) and hard (larger than $500\ \mu m$) agglomerates of silica nanoparticles, indicating the appropriateness of this approach for the processing of as-received powders. Also, it was noted that mixing two different species of nanoparticles occurred on the microscale rather than the nanoscale when using magnetically assisted nanofluidization.

According to Yu et al. [30], an oscillating magnetic field together with large magnets at the bottom of the bed could enhance nanoparticle fluidization in two ways: the disruption of large agglomerates into smaller ones, and transferring kinetic energy generated by magnetic excitation to the agglomerates due to collisions. Furthermore, it was found that the fluidization of nanopowders was considerably influenced by the mass ratio of magnetic particles, intensity, and frequency of the magnetic field.

Quevedo et al. [93] employed both vibration and magnetic assistances for the fluidization of APF and ABF nanoparticles and noted that although magnetically assisted fluidization promoted the fluidization of ABF nanopowders, a combination of these methods could result in much better fluidization behavior. This might be

plausible due the fact that by using the vibration, the contact points between particles/agglomerates and the wall of the bed were broken [21] and the detached entities then participated in the circulation path in the bed and fell down to the bed bottom, in the agglomerate breaking region using coarse and dense magnets, all causing greater fluidization quality.

However, in the case of a single magnetic aid, it could not transmit effectively in the whole bed [35]. Zeng et al. [31], [94] reported that adding hard to fluidize nanoparticles in the bed of APF behavior, resulted in the reduction of a homogeneous operating velocity range which could be compensated with the help of an external magnetic field with the correct intensity and large heavy magnetic particles stirring at the bed bottom.

Recently, Zhou et al. [95] studied the behavior of Fe_3O_4 magnetic nanoparticles in a magnetically assisted fluidized bed.

Although the magnetic nanoparticle could not be fluidized in a conventional fluidized bed, good fluidization was obtained by the addition of either a coarse steel sphere or other nonmagnetic nanopowders to the bed under the application of the magnetic field. The former acted as an agglomerate breaker and the latter as glidants to make the magnetic agglomerates more fragile, both resulted in better nanofluidization behavior.

IV.4. Electrofluidization

The investigation of the effect of an electric field on the fluidization behavior of nanoparticles has only started in recent years and research in this field is still scarce. Kashyap et al. [96], [97] studied the influence of a horizontal electric field on a bed of 10 nm silica nanopowders in a rectangular fluidized bed.

The main observation reported in their work was that the bed expansion was drastically reduced on the application of an electric field. They explained it as the result of the addition of a downward acting electric force to the gravity force.

Although this result was not appropriate in the point of gas-solid contact, the authors believed that this technique would be useful for decreasing elutriation from the fluidized bed.

Similarly, Valverde et al. [98] and Quintanilla et al. [99] found that bed expansion was hindered for 12 nm silica nanoparticles when the bed was subjected to a horizontal electric field.

From the analysis of agglomerate trajectories, Valverde et al. [98] estimated the electric charge per agglomerate and from that value, they concluded that the electrostatic force between agglomerates, which was caused by charges, was negligible as compared to van der Waals force.

Thus, it implied that the charge of nanoparticles in the bed did not affect the agglomerate size and structure. Instead, the electric field led to pushing the agglomerates toward the lateral wall of the bed, resulting in bed compaction and the appearance of a highly heterogeneous fluidization state.

Motivated by the fact that applications of an electric field and vertical vibration can reduce the entrainment and enhance the bed expansion, respectively, Quintanilla et al. [99] studied the simultaneous effect of these fields on nanofluidization. It was found that when both techniques were applied, those conflicting effects could be practically compensated.

At small amplitude vertical vibration, for which there was no bubble stimulation due to vibration, a net bed collapse from the electric field and bed enlargement from the vibration could be obtained by linear superposition of the separate effects of both fields.

At large vibration amplitude and low frequencies, which aroused bubbles by vibration, the horizontal component of agglomerate flow caused by the electric field acted against bubble formation, thus, favoring bed expansion.

Lepek et al. [29] found that a nonuniform alternating electric field along the bed height, while field strength was high at the bottom and very weak at the free surface, enhanced the fluidization of nanoparticle bed. The technique was suitable to achieve highly expanded fluidization for a particulate bed of unsieved nanopowders for which stratification is a common phenomenon in a conventional fluidized bed. They thought that the quality of nanofluidization was promoted in two ways.

On the one hand, larger agglomerates that sank to the bottom of the bed were strongly agitated by a high intensity electric field and resulted in the destabilization of gas channels close to the gas distributor to homogenize the gas distribution in the bed and, on the other hand, since small agglomerates at the top of the bed were weakly affected by the field, excessive elutriation was avoided.

Although the above-mentioned studies tried to elucidate the influence of this method on the fluidization behavior of ultrafine powders, more study is required to completely clarify unknown points of this technique.

IV.5. Use of a Centrifugal Fluidized Bed

Centrifugal fluidized beds (CFB) have many advantages over conventional fluidized beds, such as increasing the incipient fluidization velocity to hinder the onset of the unstable bubbling flow regime, preventing the elutriation of particles at relatively high gas velocities by controlling the vessel rotational speed, operating in a wide range of gas velocities leading to a much higher gas throughput per unit area of distributor, high contact efficiency between gas and solid, a smaller footprint, a thin bed resulting in either no bubbles or very tiny ones, very little gas bypassing, a shorter processing time, and a small space requirement [2], [100]-[103]. Due to these benefits, employing CFB devices has been proposed by some researchers to enhance the fluidization quality of fine/ultrafine powders.

Qian et al. [7], [101] theoretically stated that under a

centrifugal force, particles that belong to group C can shift to group A.

To confirm the theoretical study, they showed that C powders (7 μm alumina) could fluidize in a CFB operating at a sufficiently high rotating speed to shift them into group A or B.

Matsuda et al. [102], [104] found that ultrafine particles could be fluidized while forming agglomerates under high rotational acceleration G. By increasing G, the agglomerate size observed near the distributor became smaller.

Matsude et al. [34] fluidized agglomerates of nanoparticles with a primary particle size of 7 nm. They proposed an interesting energy balance model, which predicted a reduction in agglomerate size at high centrifugal forces.

However, the agglomerate size to validate the model was calculated from the data on minimum fluidization velocity and using correlations of Wen and Yu [105], rather than by direct measurements.

Employing APF and ABF nanoparticles, Quevedo et al. [2] and Nakamura and Watano [35] observed that the minimum fluidization velocities of nanopowders were linearly increased as the centrifugal acceleration increased. However, Nakamura and Watano [35] found that the bed expansion decreased with increasing G.

Also, based on measured bed expansion data and using the modified Richardson-Zaki equation coupled with fractal analysis they calculated the agglomerate size and density under different gravitational accelerations and reported that the agglomerate size decreased and its density increased by centrifugal acceleration. According to their calculations, agglomerate size and density were smaller and larger, respectively, than those found in conventional or vibration and magnetically assisted fluidized beds.

Furthermore, they found that similar to results obtained for sound, vibration, and magnetic assisted nanofluidization, when two different species of nanoparticles were fluidized in the CFB, a good degree of mixing occurred on the microscale, rather than on the nanoscale.

IV.6. Use of a Tapered Fluidized Bed

Operation in a tapered fluidized bed tends to simultaneously fluidize larger agglomerates of fine/ultrafine particles at the bottom of the bed and smaller ones at the top while preventing entrainment of smaller agglomerates from the top of the bed [36], [62]. Venkatesh et al. [36] showed that using a conical fluidized bed, with an expanding cross section along the gas flow direction, for micron size fine particles at high gas velocities led to a completely mixed fluidization with no segregation, while those particles could not be inherently fluidized in a conventional fluidized bed. Also, Tong et al. [106] employed a tapered fluidized bed to fluidize various ultrafine particles and found the bed was more effective than a conventional cylindrical one.

IV.7. Addition of Foreign Particles

The different approaches that have been discussed vary in efficiency and from a practical perspective some of them might be difficult to implement for a large scale industrial application, whereas others might not be economically feasible except for selected applications [107].

Employing external mechanical vibration and an oscillating magnetic field are some examples for this discussion [72], [107].

Also, the widely reported sound assisting method is quite successful but like the vibration and magnetic field, it is energy intensive and brings about high elutriation rates of particulate bed materials [29], [34], [107]. The addition of foreign particles to the bed is another assisting approach, which has some advantageous over other techniques, such as no need to change the column design or obtain additional equipment or devices and studies carried out on this subject can cover a wide range of particles in terms of density, size, and shape, which means different fluidization behaviors could be observed with the mixture of powders [107]-[110].

Brereton et al. [37] and Li et al. [111] investigated the possibility of operating pure silica aerogel ($dp < 20\ \mu m$) in a circulating fluidized bed with an L-valve in the external recycle section. They found that smooth circulation of pure aerogel agglomerates was not possible due to gas and solid being unable to pass through the valve.

However, by adding the correct amounts of granulate materials (Ottawa sand, $d_p = 149\ \mu m$, with sand to aerogel volume ratio ~ 4:1 and alumina particle, $d_p = 64\ \mu m$, with alumina to aerogel volume ratio ~ 1:4), much of the agglomeration was suppressed and a mixture with free flowing characteristics, ideal for contact in a circulating fluidized bed, was obtained.

In parallel with these studies, a perfectly homogeneous fluidization of Ni/SiO_2 aerogel blended with a sufficient amount of alumina particles ($d_p = 60\ \mu m$) was reported by Klvana et al. [12] and Lauga et al. [38].

Observation using the optical microscope revealed that below the appropriate level of alumina in the admixture, in addition to aerogel particles that stuck to alumina grains, there were some aerogel particles still free, which resulted in poor fluidization behavior for the mixture.

However, for mixtures having the right quantity of alumina, since there was enough available alumina surface area to collect the whole aerogel agglomerates, all of them surrounded alumina particles giving birth to hybrid particles.

Considering this concept, Lauga et al. [38] could explain the experimental findings of Brereton et al. [37]. They attributed different added volumes of the two different support particles to their equal apparent available surface for catching all aerogel particles in the bed.

Moreover, the authors recommended that appropriate support for improving the fluidization behavior of cohesive materials could be selected in light of the following conditions:

(i) The smaller the support particles, the smaller amount of these particles are required to collect the cohesive particles. However, the resultant hybrid particles should be large enough to exhibit group A characteristics.
(ii) The Liftshitz-van der Waals coefficient has to be close enough to that of cohesive particlesto promote good adhesion between the two types of particles.

Later on, Zhou and Li [112] proposed a particle agglomeration number Ae based on the force analysis between the agglomerate body and its outer-most particle.

Through the addition of a number of powders to the primary cohesive bed of SiC particles, they found that powders with $Ae \leq 40{,}000$ could be fluidized, but those with $Ae > 40{,}000$ could not.

Using this strategy they were able to find the optimum amount of addition particles in the mixture to decrease the interparticle cohesive force in the original bed and improve its fluidization behavior.

Ajbar et al. [110] reported that the addition of small proportions of group A particles could diminish the cohesiveness of type C powders and result in a more uniform fluidization.

The technique of foreign particle addition has received relatively a little attention for the fluidization of nanoparticle materials.

In 1999, Li et al. [113] observed the same phenomenon as that of Brereton et al. [37] and Li et al. [111] when they used a mixture of $CaCO_3$ nanoparticle ($d_p = 90\,nm$) with FCC particles ($d_p = 54\,\mu m$) in a circulating fluidized bed.

Song et al. [109] experimentally studied the fluidization behaviors of SiO_2 and TiO_2 nanoparticles mixed with three different size ranges and various quantities of coarse particles of FCC, ordinary Al_2O_3 and heat-resistant Al_2O_3. They found that the fluidization behavior of the mixture significantly improved with much less nanoparticle elutriation and the best results were obtained using the $60 - 85\,\mu m$ size range that corresponds to group A classification, irrespective of the material.

Similarly, enhancement in the fluidization of the hydrophilic Aerosil 200 nanoparticulate bed blended with sand particles of group A powders was reported by Ajbar et al. [107].

The authors also noted that the particle mixing approach led to much less bed entrainment compared to the sound assisting method.

It is worth mentioning that results of two later studies confirm the procedure suggested by Laugu et al. [38] through which the addition of external particles enhances the fluidization quality of cohesive powders.

IV.8. Use of Micro-Jets as a Secondary Flow in the Bed

Most recently, Quevedo et al. [22] developed a new technique by which the fluidization of nanoparticle agglomerates could be greatly enhanced. It was experimentally shown that the fluidization behavior of both APF and ABF nanopowders was significantly improved by introducing a secondary gas flow to the bed, using a downward pointing micronozzel in the form of a high velocity (hundreds of meters per second) microjet. For example, APF nanopowders expanded up to 50 times the initial bed height and ABF nanoparticles were changed to APF type, showing a bed expansion as much as 5 times the original bed height with the absence of bubbles.

Additionally, it was found that the microjet resulted in the breakup of large agglomerates, hindering channeling, curtailing bubbling, and promoting liquid-like fluidization behavior.

Moreover, the fluidization of both types of nanoparticles were accompanied by a reduction in the minimum fluidization velocity and an increase in the normalized bed pressure drop, which are proof of better fluidization quality.

Quevedo et al. [22] also studied the mixing characteristics of different nanoparticle species under the application of a microjet in the bed.

More interestingly, unlike other assisting methods, which under the best conditions could achieve microscale nanomixtures, they observed that the mixing of nanoparticle species occurred on the nanoscale.

By implementing discrete particle modeling to simulate the fluidization system employed by Quevedo et al. [22], van Ommen et al. [5] concluded that the enhancement of nanofluidization quality by microjet was caused by the size reduction of agglomerates through agglomerate-agglomerate collisions in the bed.

By fluidizing nanopowders in cylindrical beds with different sizes, when beds were assisted by microjets, Quevedo et al. [22] could reach similar results regarding the improvement of fluidization behavior of nanomaterials with this assisting method and, hence, confirm the easy scale-up of the technique.

The use of the microjet compared to other assisting techniques has the following advantages: it is efficient, simple to use, does not need expensive equipment nor foreign materials added to the bed, uses less energy, is easily scaled-up and can be used to blend different species of nanoparticles on the nanoscale to form nanocomposities [4].

These priorities lead to a high potential of utilization of this method for fine or nanoparticle fluidization for their various industrial applications in the near future.

Finally, to have a quick review of different assisting methods for improving the fluidization quality of fine/ultrafine particles, Table III provides a summary of the advantages and limits of these approaches.

TABLE III
SUMMARY OF ADVANTAGES AND LIMITS OF DIFFERENT ASSISTING METHODS FOR IMPROVING THE FLUIDIZATION QUALITY OF FINE/ULTRAFINE PARTICLES

Method	Advantageous	Limits
Acoustic wave	Channeling and slugging are eliminated. Minimum fluidization velocity decreases. Agglomerate size decreases. Elutriation rate decreases.	It is energy intensive. Decrease in elutriation loss is not appreciable. Operation outside the optimal ranges of SPL and f_s, not only won't improve the fluidization quality, but also deteriorates it. Operating problem with the presence of sound with high SPL. Mixing of different nanoparticles could be achieved up to microscale.
Vibro-fluidization	Channeling and slugging are eliminated. Bed pressure drop increases. Minimum fluidization velocity decreases. Agglomerate size decreases. Elutriation rate decreases.	It is energy intensive. Decrease in elutriation loss is not appreciable. Bubbles would arise at high vibration intensity. Processing of as-received fine/ultrafine particles by this approach is not feasible. Mixing of different nanoparticles could be achieved up to microscale.
Magnetically assisted fluidization	Fluidization of completely defluidized bed would be feasible. Minimum fluidization velocity decreases. Size of bubbles in bubbling fluidization regime of some micron size fine particles decreases. Elutriation rate decreases.	It is energy intensive. Decrease in elutriation loss is not appreciable. when large and dense magnets are used: The magnets mostly present at the bed bottom and the magnetic aid cannot transmit effectively in the whole bed. when ferro-magnetic particles with size and density similar/close to those of bed material are used: The magnets act as foreign particles and acceptance of these particles in the process is the main question.
Electrofluidization	Bed expansion increases in the case of nonuniform alternating electric field along the bed height. Elutriation rate decreases.	Bed expansion decreases and highly heterogeneous fluidized bed appears in the case of horizontal electric field.
The use of a centrifugal fluidized bed	Minimum fluidization velocity decreases. Agglomerate size decreases, smaller than those attainable by assisting the bed with acoustic, magnetic and electric fields, and mechanical vibration. Elutriation rate decreases.	Bed expansion decreases. Mixing of different nanoparticles could be achieved up to microscale. Powerful compressor is needed to supply the required fluidizing medium. Attrition is a harmful problem for this type of fluidized beds.
The use of a tapered fluidized bed	Simultaneously fluidizes large agglomerates at the bed bottom and small agglomerates at the top of the bed. Elutriation of small agglomerates is hindered.	Not reported.
Additional of foreign particles	There is no need to change the column design or obtain additional equipment. Elutriation rate decreases. Makes circulating fluidization mode of ultrafine particle agglomerates possible.	Acceptance of the presence of foreign particles in the process is under the question.
The use of micro-jet as secondary flow	Channeling is hindered. Bed pressure drop increases. Minimum fluidization velocity decreases. Bed expansion increases, much higher than those obtained by other techniques. Agglomerate size decreases. The fluidization characteristics of ABF powders change into APF ones. Mixing of different nanoparticles could be achieved up to nanoscale. It is easy to scale-up.	Not reported.

V. Experimental Techniques for Measuring Agglomerate Size

Fine/ultrafine powders tend to form agglomerates when exposed to a gas flow greatly exceeding the minimum fluidization conditions of primary particles in a gas-solid fluidized bed. Thus, agglomerates are the entities that fluidized in the bed, not the individual particles, and hence it is essential to measure the size, shape, and density of the agglomerates under different operating conditions to increase understanding of fluidization behavior of these powders [75].

Among all properties of agglomerates, their mean size, which depends on the physical properties and chemical composition of the primary particles, as well as the presence of external cohesive forces due to electrostatic effects, liquid bridge, etc., is an important factor in determining the quality of fluidization, that is, whether the fine/ultrafine particle will fluidize as APF or ABF [114], and for the performance of heat and mass transfers since particle agglomeration reduces the available fluid-solid contact area [82]. Due to the fragile nature of the agglomerates and the time-dependent process of dynamic equilibrium, the measurement of the agglomerate size poses significant challenges for the development of sampling method [47], [82].

In past years, several works have focused on determining the size of fine/ultrafine particle agglomerates. Pacek and Nienow [18] developed a technique called the "freezing method", in which the agglomerates were frozen by spraying a binder solution of wax from the top of the bed before sampling to facilitate analysis by scanning electron microscopy (SEM).

SEM analysis was also applied to agglomerates sampled directly from the fluidized bed by adhesive tape [17], [20] or aspiration [32]. In addition, agglomerates of fine particles were extracted from the bed by adhesion to a sheet of paper [41], [115]. The principal issue concerning these approaches is that the agglomerates, especially nanoparticles, are very porous and fragile, and might be broken during their removal from the bed and/or during sampling preparation for the SEM analysis [32]. Thus, intrusiveness, which might affect the agglomerate properties, is the main difficulty for these techniques.

To avoid the serious problem of sample deformation during SEM measurements, another technique, called Particle/Droplet Image Analysis (PDIA) for the direct and dynamic measurement of the agglomerate size in the splash zone of the fluidized bed was developed [1], [21], [30], [32], [75], [116], [117]. In this technique a laser is used to illuminate the free board and the region close to the upper surface of the solid bed from behind, and shadow images of agglomerates are taken with a specially calibrated camera.

Although this technique has the advantage of being dynamic and noninvasive, it is not known whether the mean agglomerate size measured in the lean section of the fluidized bed is actually representative of the mean agglomerate size in the bed itself [4]. In other words, the efficiency of the technique can be limited by stratification of agglomerates due to size dispersion, which is a common phenomenon for ABF particles, and the agglomerate samples recorded in the images close to the bed free surface could be biased towards smaller sizes [118].

An obvious limitation for the above-mentioned techniques is that they are only capable of measuring the agglomerate size in the top bed. To compensate for the deficiency of these methods, Xu and Zhu [47] developed an "online sampling technique", as depicted in Figs. 6, which, it was claimed, is capable of sampling the agglomerates, without disrupting their sizes or structures from any parts of the bed (top, middle or bottom bed). The agglomerates are sampled in situ using a sampling idle from the top of the bed without stopping the fluidizing gas. For sampling the agglomerates in the upper layer of the bed, the idle is directly employed to pick up the agglomerates.

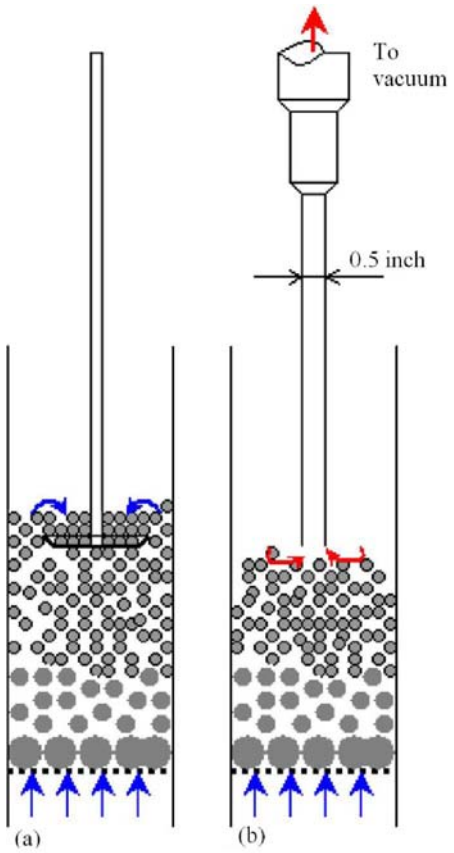

Figs. 6. Diagram of the "online sampling technique": (a) sampling the agglomerates from the top layer of the bed; (b) removing the agglomerates from the upper layer by vacuum prior to sampling for the agglomerates on the lower layer. Adapted from [47]

To sample the agglomerates in the middle and bottom of the bed, an intensity-controllable vacuum is used to remove all the particulate materials above the sampling plane before taking samples with the sampling idle. After sampling, the properties of the agglomerates can be measured using SEM.

To keep in mind the time-dependent process of dynamic equilibrium, agglomerate samples should be taken after a certain length of time when the bed is stabilized regarding the agglomerate size and shape under certain fluidization conditions. Although this is a promising technique for determining the agglomerate size at different levels of the bed, its result will not be reliable if particular care is not be taken during sampling removal by idle or discharging the above layers of the sampling plane by vacuum.

As a more efficient technique, the X-ray imaging method was developed to allow fluidized beds to be studied at length scales down to 400 nm and temporal resolutions of 1ms, with the advantage of studying the bulk of the fluidized bed in an in situ, nonintrusive, and dynamic manner [54], [119], [120]. Unlike other available imaging methods, which are usually surface techniques, X-ray microtomography imaging allows us to see through the sample and reconstruct a three dimensional internal structure of the sample. Considering this ability, the authors showed that, by using this approach, it is feasible to dynamically and nondestructively determine the agglomerate size, density, and porosity, inter-agglomerate voidage, and local solid fraction, which are nearly all required information for uncovering the physics behind the fine/ultrafine particle fluidization.

In addition, using high resolution X-ray imaging and the microtomography technique, changes in the agglomerate structure and density with different operating conditions can be easily seen. However, even though the technique seems to be a powerful one on the subject, it needs further development in order to respond to the low X-ray energies required for some fine powder samples.

Most recently, Quevedo and Pfeffer [114] introduced a new method through which in situ agglomerate size measurements and the imaging of fluidized nanoagglomerates were achieved by reducing the electric charge in the bed and using Focused Beam Reflectance Measurement (FBRM) and Particle Vision Measurement (PVM) probes. The probes successfully characterized the number weighted and volume weighted agglomerate size distributions for both APF and ABP type nanoparticles. The FBRM data and PVM images showed that the probes were capable of differentiating between different types of nanoparticles (APF and ABF) and could also evaluate the effects of the microjet assisting method on the agglomerate concentration and size.

Although this is a useful approach for measuring the agglomerate size and concentration, it suffers from the interference of the probes (19 and 25 mm I.D.) with the flow around them.

VI. Models for the Prediction of Agglomerate Size

Due to high importance of agglomerate size in the fluidization of fine/ultrafine particles, several models have been proposed to predict this parameter on the basis of the physical understanding of particle agglomeration dynamics.

These models are classified into either force [15], [112], [118], [121]-[124] or energy [17], [34], [47], [71] balances around individual agglomerates, or the use of the modified Richardson-Zaki equation [1], [20], [32], [41], [115].

VI.1. Force Balance

Chaouki et al. [15] assumed that the drag force due to gas flow, which is approximately equal to gravitational force acting on an agglomerate, is equal to the van der Waals force between primary particles.

Their model can be expressed as follows:

$$\frac{g(\rho_a-\rho_f)\pi {d_a}^3}{6} = 25\pi\mu\, u_{mf}\, d_a\, \frac{(1-\varepsilon_c)}{{\varepsilon_c}^3} = \\ = \frac{h\bar{\omega}}{8\pi Z^2}\left(1+\frac{h\bar{\omega}}{8\,\pi^2\, Z^3\, H_r}\right) R_{as} \tag{13}$$

where ε_c is the bed voidage at agglomerate minimum fluidization velocity u_{mf}, and ρ_a and d_a are the agglomerate density and size, respectively. For proper application of Eq. (13), the authors suggested that the particle asperity radius R_{as} with a typical order of $0.1\ \mu m$ should be taken into account.

Also, they postulated that since, for agglomerate fluidization, the fixed bed breaks into pieces, the agglomerate density is fairly equal to the aerated bulk density of the primary particles. Albeit the aerogel particles, which were used in their experimental work, were closer to nanoparticles than to classical group C powders, the proposed model is also capable of predicting the agglomerate size for type C fine cohesive powders.

Iwadate and Horio [121] presented a force balance model by taking into account bubbling dynamics to predict the agglomerate size in a bubbling fluidized bed of cohesive particles. In their model, the bed expansion force caused by bubbles was balanced by the agglomerate-to-agglomerate cohesive rupture force, which was approximated by van der Waals force between two spherical porous bodies.

Based on the following model:

$$d_a = \frac{n_{k,mf}\, H_a\, (1-\varepsilon_a)}{12\pi\, Z^2\, D_b\, \rho_a\, g\, (-P_s)} \tag{14}$$

where D_b is the bubble diameter, P_s is the dimensionless particle pressure, $n_{k,mf}$ is the coordinate number of agglomerates at minimum fluidization velocity, H_a is the Hamaker constant, which is equal to $4h\bar{\omega}/3\pi$, and ε_a is the agglomerate voidage, which was measured by mercury porosimetry.

Typical values for the bed of TiO_2 fine particles were suggested to be $H_a = 0.39 \times 10^{-19}\, J$, $n_{k,mf} = 4.49$, $Z = 4A^o$, and $P_s = -0.0515$.

It should be noted that this model can only be used when the bed is bubbling and its application for uniform non-bubbling fluidization generally observed for APF nanoparticles is highly questionable.

Zhou and Li [112], [122] assumed that an equilibrium agglomerate size of cohesive particles in a fluidized bed can be estimated when the joint action of the collision

and drag forces is balanced by the buoyant weight and the cohesive force as in the following:

$$(Kinetic\ or\ drag\ force) + (collision\ force) = (gravitational\ force - bouyacy\ force) + (cohesive\ force)$$

According to this balance, they arrived at a quadratic equation to be used for finding the agglomerate size as follows:

$$-\left[\begin{array}{c}(\rho_a - \rho_f) g\, {d_a}^2 + \\ 0.33\, \rho_f\, {u_0}^2\, \varepsilon^{-4.8} + \\ + \dfrac{0.996}{\pi}\left(\dfrac{\pi\, V^6\, {\rho_a}^3}{k^2}\right)^{1/5}\end{array}\right] d_a + \frac{H_a}{4\pi\, Z^2} = 0 \quad (15)$$

where k is a function of Poisson's ratio and Young's modulus ($= 3.0 \times 10^{-6}\ Pa^{-1}$), and V is the relative velocity of agglomerates estimated by:

$$V = \left(1.5\, \overline{P_{s,n}}\, D_b\, g\varepsilon\right)^{0.5} \quad (16)$$

where $\overline{P_{s,n}}$ is the dimensionless average particle pressure of a non-sticky system, was taken to be 0.077. Zhou and Li [112] found that the density of agglomerates of micron and submicron particles was larger than the aerated bulk density of primary particles by a factor of 1.15, but smaller than the tapped bulk density, about 0.85 times the tapped bulk density. Through the analysis of the model, Zhou and Li [122] reported that higher gas velocity and fluid density, lower particle adhesion, and the collision between agglomerates are effective for agglomerate size reduction. As pointed out by Yang [62], the authors used a constant drag coefficient around the agglomerate, an assumption that is only valid for the high Reynolds number (turbulent flow), and compared the results of the model with experiments for which the Reynolds number around the agglomerates was very low (viscous flow). Accordingly, this model cannot be applied for nanoparticle fluidization in which fluidization is occurring at a creeping flow. A predictive equation to find the agglomerate size in a fluidized bed of micron size cohesive particles was proposed by Castellanos et al. [123] through studying the limit of mechanical stability of the agglomerate suspended in the gas flow field. Their predictive equation stemmed from a local force balance between shear and adhesion forces on a particle at the outer layer of the agglomerate. In the fluidized bed of micron size primary particle agglomerates, particles tend to form agglomerate due to the action of the interparticle attractive force. Besides this, the weight of the agglomerate, which is a body force acting uniformly through the agglomerate, is balanced by a hydrodynamic drag force, which acts mainly at the surface of the agglomerate because of the flow screening effect. Consequently, shear forces distributed across the agglomerate grow as the agglomerate size increases, and eventually curtails its growth. The authors suggested that the response of the agglomerate resembles that of a spring subjected to a typical strain:

$$\gamma_s \sim \frac{N_a\, m_p\, g}{K_c\, R_a} \quad (17)$$

where N_a is the number of particles in the agglomerate, m_p is the particle mass, K_c is the agglomerate spring constant, and R_a is the agglomerate radius. The agglomerate spring constant was given by $\xi / {k_a}^{\theta}$, where ξ is the interparticle attractive force constant, k_a is the ratio of the agglomerate size d_a to particle size d_p, and θ is the elasticity exponent, $\theta = 3$ was considered for a three dimensional case. In this context, the local shear force F_s acting on the agglomerate was estimated as follows:

$$F_s \sim \xi \gamma_s\, \frac{d_p}{2} \sim N_a\, m_p\, g\, {k_a}^2 \quad (18)$$

Considering the just presented concept, the particles would continue adhering to the agglomerates as long as the interparticle attractive force F_{IPF} is larger than F_s. Therefore, based on this method, the condition $F_{IPF} = F_s$ results in a criterion by which the agglomerate size can be predicted as follows:

$$Bo_g \sim {k_a}^{D_a+2} \quad (19)$$

where Bo_g is the granular Bond number, which is the ratio of the interparticle attractive force to particle weight ($Bo_g = F_{IPF}/m_p\, g$), and $D_a = \frac{\ln N_a}{\ln k_a}$ which is the fractal dimension of the agglomerate, was taken to be 2.5 similar to the diffusion-limited-agglomeration model introduced by Witten and Sander [125].

Experimental results of Castellanos et al. [41] showed that D_a for micron size agglomerates was a robust parameter and was always about 2.5, which confirms this choice.

Finally, through this criterion the agglomerate size is expressed as follows:

$$d_a = d_p \left(\frac{F_{IPF}}{(1/6)\pi\, \rho_p\, g\, {d_p}^3}\right)^{1/(D_a+2)} \quad (20)$$

The difference between this force balance with the one developed by Chaouki et al. [15] is that the former is a balance between shear and cohesion forces on the agglomerate in the local scale, while in the latter, the local interparticle attractive force was equated to the global drag force on the agglomerate [118].

As previously mentioned, the essential difference between agglomerates of micron size particles and those for APF nanoparticles is that the former forms simple agglomerates from primary fine particles, whereas the

latter, as was studied by Yao et al. [20], possesses multistage agglomeration starting from the primary nanoparticle, passing through the three dimensional chain-like structure, simple and complex agglomerates, each of the three were shaped from many components of the previous stage.

Postulating the limits to the agglomeration of simple agglomerates to complex agglomerates in the fluidized bed of nanoparticles is governed by the same physical mechanism as for fine micron size particles, Valverde and Cantellanos [124] proposed a new criterion similar to Eg. (19) for the case of nanoparticles as follows:

$$Bo_g^* \sim (k^*)^{D^*+2} \tag{21}$$

where $Bo_g^* = F^*/(N_s\, m_p\, g)$ is the ratio of the cohesive force between simple agglomerates to the weight of the simple agglomerate, N_s is the number of primary nanoparticles in each simple agglomerate, k^* is the ratio of complex agglomerate size d^{**} to simple agglomerate size d^* ($k^* = d^{**}/d^*$), $D^* = \ln N^*/\ln k^*$ is the fractal dimension of the complex agglomerates, and N^* is the number of simple agglomerates in the complex agglomerate.

Also, they considered $F^* = F_{vdw}$. By assuming a reasonable value for simple agglomerate size, even though they could have good results with this criterion for different nanoparticles, this approach has two main problems in practice.

First, the size of simple agglomerates has to be known a priori and, second, it does not account for previous stages of formation of 3D chain-like structures and simple agglomerates [118].

To compensate for these deficiencies, Valverde and Cantellanos [118] came up with a new and simple model for calculating the agglomerate size of nanoparticles by merely knowing the primary particle size and density, fractal dimension, and attractive force. They proposed to use Eq. (19) for each one of the steps of formation of nanoparticle agglomerates.

In addition, they assumed that different agglomeration stages has the same fractal dimension equal to global fractal dimension $D_a = 2.5$. Experimental results of Wang et al. [117] and Nam et al. [32] confirmed this assumption.

On the basis of these hypotheses and considering the general fractal dimension $D_a = \ln N_a/\ln k_a$, where, in the case of nanoparticles, N_a is regarded as the total number of primary particles in the complex agglomerate and $k_a = d^{**}/d_p$ as the ratio of the complex agglomerate size to primary nanoparticle size, the following correlation for the prediction of complex agglomerate size was achieved:

$$d^{**} = {d_p}^{D_a(D_a+1)/(D_a+2)^2} (2R_{as})^{(D_a+4)/(D_a+2)^2} \Lambda^{-1/(D_a+2)} {Bo_g}^{(D_a{}^2+6(D_a+2))/(D_a+2)^3} \tag{22}$$

where $\Lambda = g_{ef}/g$ is the ratio of effective acceleration g_{ef} to gravitational acceleration, which is an important parameter for centrifugal and vibro-fluidized beds, and Bo_g is the nanoparticle Bond number calculated as the ratio of attractive force between primary nanoparticles to the weight of the primary nanoparticles, defined as follows:

$$Bo_g = \frac{F_{IPF}}{(1/6)\pi\, \rho_p\, g\, {d_p}^3} \tag{23}$$

Interparticle attractive force between primary nanoparticles F_{IPF} was considered as the summation of van der Waals and capillary forces ($F_{IPF} = \frac{H_a\, d_p}{24\, Z^2} + \frac{\pi\gamma\, d_p}{2}$) to cover both hydrophobic and hydrophilic nanoparticles.

Also, the interparticle attractive force between three dimensional chain-like structures and simple agglomerates was equated to van der Waals force, considering $R_{as} = 0.1\ \mu m$, as in the following:

$$F_{vdw-II} = \frac{H_a\, R_{as}}{12\, Z^2} \tag{24}$$

Eq. (24) is another correlation that has been used by some authors to calculate the van der Waals force between two hard spherical particles ($H_r \gg$). Eq. (7), which is a more general correlation for the computation of van der Waals force, is equal to Eq. (24) for hard particles and considering $H_a = 4h\bar{\omega}/3\pi$.

In order to discriminate the van der Waals force estimated by Eq. (24) to that of Eq. (7), we symbolize the force as F_{vdw-II} in Eq. (24).

It is worth mentioning that Eq. (22) predicts that the agglomerate size should not depend essentially on the properties of the environmental gas, like gas viscosity. This was experimentally checked by Valverde et al. [126] in which they used different gases as fluidizing medium for nanoparticles and found that the gas type had negligible effect on the agglomerate size.

VI.2. Energy Balance

Following similar reasoning to Chaouki et al. [15], Morooka et al. [17] assumed that the agglomerate will disintegrate if the collision energy is greater than the energy that is required to break the agglomerate into two parts (i.e., the energy due to the interparticle forces). Employing this philosophy, the equilibrium size of agglomerates can be calculated by:

$$(energy\ generated\ by\ laminar\ shear) + (kinetic\ energy\ of\ agglomerate) = = (energy\ required\ to\ break\ up\ the\ agglomerate)$$

$$3\pi\mu\, u_{mf}\, {d_a}^2 + \left(\frac{\pi}{6}\right)\rho_e\, {d_a}^3 \left(\frac{{u_{mf}}^2}{2}\right) = E_{break} \tag{25}$$

where ρ_e is the density of the emulsion phase in the fluidized bed and E_{break} is the energy needed to disrupt the agglomerate, which is given as:

$$E_{break} = \left(\frac{\pi}{2}\right) {d_a}^2 \sigma\, Z \tag{26}$$

where Z is the distance at which van der Waals force is maximized and, as previously mentioned, is approximately equal to 4 A^o, and σ is the maximum tensile strength, which can be approximated using the Rumpf [127] theory, supposing that forces are transmitted at coordinate points of particles forming the agglomerate:

$$\sigma = \frac{(1-\varepsilon_a)}{\varepsilon_a\, {d_p}^2}\, F_{IPF} \tag{27}$$

Agglomerate voidage ε_a was approximated by $1 - \rho_a/\rho_p$. Since they carried out their experiments in a dry environment, van der Waals force was dominant over other types of interparticle forces and, hence, $F_{IPF} = F_{vdw}$.

Using Eqs. (7), (26), and (27), E_{break} can be expressed as follows:

$$E_{break} = \frac{{d_a}^2\, h\bar{\omega}\, R_{as}}{16\, Z\, {d_p}^2} \left(\frac{1-\varepsilon_a}{\varepsilon_a}\right) \left(1 + \frac{h\bar{\omega}}{8\,\pi^2\, Z^3\, H_r}\right) \tag{28}$$

Although this model paved the path for using energy balance modeling to estimate the agglomerate size, Zhou and Li [112] believed that the first term in left hand side of Eq. (25), which is related to energy generated by laminar shear, should not be involved in the total energy balance and also it was not true to use the minimum fluidization velocity as the characteristic velocity of agglomerates.

Similar criticism concerning the inappropriateness of employing the minimum fluidization velocity as the relative velocity between two agglomerates was highlighted by Xu and Zhu [47].

In a centrifugal fluidized bed of nanoparticles, Matsuda et al. [34] presented an energy balance equation based on attainable energy and agglomerate disintegration energy.

They assumed that there exists an attainable energy E_a for the disintegration of agglomerates proportional to ${g_{ef}}^r$ and r was adjusted to 0.4 to fit the model to their experimental results. For the basis of their model, they modified the agglomerate disintegration energy presented by Morooka et al. [17] by considering that energy consumption for breaking powder should consider the energy required per unit-weight of agglomerate, rather than only focusing on the disintegration of a given agglomerate. This is due to the fact that the required energy for agglomerate disruption increases as the agglomerate size decreases.

Accordingly, the energy consumption for the disintegration of agglomerate per unit-weight of agglomerate E_{dw} was described by using the density of agglomerate as in the following:

$$E_{dw} = E_{break}\, \frac{1}{(1/6)\pi\, \rho_a\, {d_a}^3} = \\ = \frac{3\, h\bar{\omega}\, R_{as}}{8\pi Z \rho_a d_a {d_p}^2} \left(\frac{1-\varepsilon_a}{\varepsilon_a}\right) \cdot \\ \cdot \left(1 + \frac{h\bar{\omega}}{8\,\pi^2\, Z^3\, H_r}\right) \tag{29}$$

and by substituting (ρ_a/ρ_p) into $(1-\varepsilon_a)$, Eq. (29) reforms as:

$$E_{dw} = \frac{3\, h\bar{\omega}\, R_{as}}{8\pi Z\, (\rho_p - \rho_a)\, d_a {d_p}^2} \left(1 + \frac{h\bar{\omega}}{8\,\pi^2\, Z^3\, H_r}\right) \tag{30}$$

In this context, by considering $E_a = c_a\, \Lambda^{0.4}$, where c_a is a parameter that depends on the operating conditions and experimental apparatus design, the disintegration of agglomerates occurs when $E_a > E_{dw}$ and stops when E_a is equivalent to E_{dw}. Consequently, the size of the agglomerate can be expressed as the following when $E_a = E_{dw}$:

$$d_a = \frac{3\, h\bar{\omega}\, R_{as}}{8\pi Z\, c_a (\rho_p - \rho_a)\, {d_p}^2\, \Lambda^{0.4}} \left(1 + \frac{h\bar{\omega}}{8\,\pi^2\, Z^3\, H_r}\right) \tag{31}$$

The main critique regarding this model is that the agglomerate size to validate the model was calculated from the data on minimum fluidization velocity and using correlations of Wen and Yu [105], rather than by direct measurements.

Xu and Zhu [47] and Guo et al. [71] used the energy balance strategy and proposed models to predict the agglomerate size in the case of assisting fluidization using external fields, such as the vibration and acoustic field.

The general form of energy balance was expressed as, the agglomerate tends to break down when the total energy due to collision E_{coll} and the external field E_{ext} exceeds the energy due to the cohesion E_{coh}. In this regard, the general energy balance is given by:

$$E_{coll} + E_{ext} = E_{coh} \tag{32}$$

Xu and Zhu [47] used the following correlation to calculate the collision energy:

$$E_{coll} = 0.104\pi\, \rho_a {d_a}^3\, V^2 \tag{33}$$

They believed that employing Eq. (16) for calculating the relative agglomerate velocity, which was proposed by Zhou and Li [112], [122], or replacing it by the minimum fluidization velocity, following Morooka et al. [17], are

not appropriate ways to estimate the relative velocity of agglomerates. This is due to the fact the using Eq. (16) results in the relative velocity being as high as the gas velocity, and in some cases even much higher than that, and employing the second approach yields overlooking the effect of the superficial gas velocity on the agglomerate size. In this regard, the authors approximated V as:

$$V = 0.1\sqrt{u_0\, u_{mf}} \tag{34}$$

Also, the contribution of vibration, as the external field, in breaking agglomerates was expressed as:

$$E_{ext} = E_{vib} = \frac{0.01\,\pi^3}{3}\,\rho_a {f_v}^2 {A_m}^2 {d_a}^3 \tag{35a}$$

Finally, by using the energy balance the agglomerate size was given as follows:

$$d_a = \frac{\frac{\pi}{96}\,1.61\,{\varepsilon_a}^{-1.48}\,\frac{1-\varepsilon_a}{\varepsilon_a}\,\frac{H_a}{d_p}\,\frac{1}{Z}}{0.104\pi\,\rho_a\,V^2 + \frac{0.01\,\pi^3}{3}\,\rho_a {f_v}^2 {A_m}^2} \tag{35b}$$

A comparison between the results of the model and experiments for beds of micron size fine particles, while agglomerate size were measured by an "online sampling technique," showed the acceptable accuracy of the model. Albeit this model was validated for micron size particles, it is also capable of predicting the agglomerate size of nanoparticles, as well.

Considering the energy given by the external field as sound wave energy E_{sou}, and the presence of critical values for sound frequency f_{sc} and sound pressure level SPL_c, as discussed in section 4.1, and using the general energy balance like Eq. (32), Guo et al. [71] could achieve the following equation to predict the agglomerate size for beds of submicron and nanoparticles:

$$d_a = \{\left(h\bar{\omega}/16Z{d_p}^2\right)((1-\varepsilon_a)/\varepsilon_a)\cdot \\ \cdot (1 + h\bar{\omega}/8\,\pi^2\,Z^3\,H_r) \pm (\pi/4)k_{at}10^{-12+SPL}\cdot \\ \cdot\, e^{(SPL-SPL_c)/SPL_c}\} \,/\, 0.104\pi\,\rho_a\,V^2 \tag{36a}$$

where k_{at} is the attenuation coefficient, which is a function of the sound frequency ratio and the sound pressure ratio as in the following:

$$k_{at} = f\left(\frac{f_s}{f_{sc}}, \frac{SPL - SPL_c}{SPL_c}\right) \tag{36b}$$

VI.3. Modified Richardson-Zaki Equation

Fitting the bed expansion data to the modified Richardson-Zaki (R-Z) empirical equation is another method that has been used to obtain information about the agglomerate size.

Originally, the R-Z equation was developed to describe the bed expansion behavior of homogeneous liquid-solid fluidized beds.

However, it was found that the equation can be also applied for smooth fluidization of a non-cohesive gas-solid system and takes the form:

$$\frac{u_0}{u_{p0}} = (1-\emptyset)^n \tag{37}$$

where u_0 is the superficial gas velocity (which for uniform fluidization must be equal to the initial settling velocity u_s in sedimentation), $\emptyset$ is the particle volume fraction, the R-Z exponent n is close to 5.0 for the Stokes-flow regime, and u_{p0} is the terminal velocity for a single particle, expressed by:

$$u_{p0} = \frac{\rho_p\, g\, {d_p}^2}{18\,\mu} \tag{38}$$

By using the R-Z equation for fine cohesive particles in a homogeneous fluidization regime, Valverde et al. [115] found that the terminal settling velocity of fluidizing entities was higher than the terminal velocity of a single particle, which indicated the agglomerate fluidization for those particles.

Thus, it was noted that for the case of agglomerate fluidization, the terminal settling velocity of agglomerate u_{tsa} rather than the velocity for the primary particle should be used in the R-Z equation, which introduced the first modification of this equation. It should be taken into account that the R-Z equation is only valid for APF beds since the superficial gas velocity is equal to the initial settling velocity. While for ABF beds, since u_0 is appreciably larger than u_s due to the bypass of a substantial volume of gas by bubbles, the R-Z equation cannot be applied [1], [4], [41], [115], [124].

Considering these issues, to predict the agglomerate size, Yao et al. [20] fitted their bed expansion experimental data of APF nanopowders to the modified R-Z equation:

$$\frac{u_0}{u_{tsa}} = (1-\emptyset)^n \tag{39}$$

Consequently, they could obtain the fitting parameters u_{tsa} and n from experimental results.

To calculate the agglomerate size from these data, similar to Chaouki et al. [15], they approximated the agglomerate density to the bulk density of the primary nanoparticles and employed the following correlation for terminal settling velocity of the agglomerate:

$$u_{tsa} = \frac{\rho_a\, g\, {d_a}^2}{18\,\mu} \tag{40}$$

Although the proposed method is much simpler than the force and energy balance modeling approaches and requires much fewer parameters to be estimated or fitted, it has a major inconvenience.

The problem concerning the Yao et al. approach is that they obtained values of n as low as 3, while since the Reynolds number for nanofluidization is typically very small [1], the R-Z exponent cannot deviate too much from $n \approx 5$. As pointed out by Valverde and Castellanos [118], this problem originates from neglecting the screen effect of agglomerates.

Thus, the next modification on the R-Z equation was to consider the gas flow screening by agglomerates.

In order to implement the second modification, Valverde et al. [115] and Castellanos et al. [41] assumed that the agglomerates behave like hard spheres with a hydrodynamic radius equal to their radius of gyration, thus it was possible to use the agglomerate volume fraction $\emptyset_a$ instead of the particle volume fraction $\emptyset$ in the modified R-Z equation as follows:

$$\frac{u_0}{u_{tsa}} = (1 - \emptyset_a)^n \tag{41}$$

Agglomerates of fine particles have fractal structures [32], [41], [115] for which a number of primary particles in the agglomerate N_a can be approximated by the following:

$$N_a = {k_a}^{D_a} \tag{42}$$

where k_a is the ratio of the agglomerate size d_a to primary particle size d_p, and D_a is the fractal dimension. In this regard, the terminal settling velocity of agglomerate relates to the terminal velocity of the primary particle as follows:

$$u_{tsa} = \frac{u_{p0}\, N_a}{k_a} \tag{43}$$

and agglomerate volume fraction to particle volume fraction as:

$$\emptyset_a = \frac{\emptyset\, {k_a}^3}{N_a} \tag{44}$$

Substituting Eqs. (43) and (44) in Eq. (41) yields:

$$\frac{u_0}{u_{p0}} = \frac{N_a}{k_a}\left(1 - \emptyset \frac{{k_a}^3}{N_a}\right)^n \tag{45}$$

By using this approach and fitting the bed expansion experimental data of APF nanoparticles to Eq. (45), fitting parameters and, hence, N_a and k_a are determined. Accordingly, agglomerate size can be calculated by $d_a = k_a \times d_p$.

In addition to agglomerate size, it is possible to determine the agglomerate density and inter-agglomerate voidage, which are advantages of this method. This approach was used by Nam et al. [32] for the nanoparticle fluidized bed and it could accurately predict the agglomerate size in comparison with the measured data by employing a laser-based planar imaging analysis carried out for images at the splash zone of the bed.

They have also reported that with n values in the range of 4 to 6, the fractal dimension, number of primary particles, and diameter of the agglomerates were insensitive to the value of the R-Z exponent n.

Zhu et al. [1] tried to solve this problem by postulating that the density of the agglomerate remains almost constant before ρ_{a0} and during fluidization. A combination of this assumption with an overall mass balance on the powder in the fluidized bed, by ignoring the elutriation and particle adhesion to the walls of the column, yields:

$$\varepsilon = 1 - \frac{H_0}{H}(1 - \varepsilon_0) \tag{46}$$

where H_0 is the fixed bed height, H is the bed height during fluidization, and ε_0 is the fixed bed voidage.

By considering Eq. (39), but in the form of bed voidage as in the following:

$$\frac{u_0}{u_{tsa}} = \varepsilon^n \tag{47}$$

Eq. (46) reforms as:

$${u_{tsa}}^{1/n} - {u_{tsa}}^{1/n}(1 - \varepsilon_0)\frac{H_0}{H} = {u_{tsa}}^{1/n} \tag{48}$$

By drawing a plot of ${u_{tsa}}^{1/n}$ vs. H_0/H and forming a linear regression for experimental bed expansion data of APF powders, the terminal settling velocity of agglomerate u_{tsa} and the bed voidage at fixed bed ε_0 can be determined. Accordingly, the agglomerate density before/during fluidization can be estimated as follows:

$$\rho_a = \rho_{a0} = \frac{\rho_b}{(1 - \varepsilon_0)} \tag{49}$$

and, finally, the agglomerate size can be calculated from Stokes law, Eq. (40). Zhu et al used $n = 5.0$ in their calculation, since the flow was in creeping motion, and found that while their approach was simpler than that of Nam et al. [32], the predictions of both approaches were very close to each other. Moreover, the authors showed that the prediction of their model was fairly well compared to the agglomerate size measured by the in situ optical measurement technique on the lean zone of the fluidized bed. Results of the calculation of agglomerate size using different models reviewed in this section together with the physical properties of applied powders are summarized in Table IV.

TABLE IV
RESULTS OF THE CALCULATION OF AGGLOMERATE SIZE USING DIFFERENT PREDICTIVE MODELS

Source	Trade no.	Material	d_p (μm)	ρ_p (kg/m^3)	Fluidization aid	Calculated d_a (μm)
Chaouki et al. [15]		Cu/Al_2O_3 aerogels	<0.01	1200 - 1500		245 - 264
Morooka et al. [17]		Si_3N_4	0.13	2910		350
Iwadate and Horio [121]		TiO_2	0.27	4250		172
Zhou and Li [112, 122]		SiC	1.82	3210		635
		TiO_2	0.6	3880		529
		SiO_2	4.6	2000		330
Yao et al. [20]	R812s	SiO_2	0.007	2560		230
	TS530	SiO_2	0.009	2560		277
	R504	SiO_2	0.012	2560		238
	R972	SiO_2	0.016	2560		277
	Aerosil 300	SiO_2	0.007	2560		286
	Aerosil 150	SiO_2	0.014	2560		331
Matsuda et al. [34]		TiO_2 Hydrophilic	0.007	4000	Centrifugal field	
					$\Lambda = 9.1$	239
					$\Lambda = 25.2$	159
					$\Lambda = 82.5$	99
Nam et al. [32]	R974	SiO_2 Hydrophobic	0.012	2200	Vibration	160
Zhu et al. [1]	R974	SiO_2 Hydrophobic	0.012	2560		211
	R805	SiO_2 Hydrophobic	0.012	2560		279
	R104	SiO_2 Hydrophobic	0.012	2560		245
	R711	SiO_2 Hydrophobic	0.012	2560		207
	COK84	SiO_2-Al_2O_3: 7-1	0.012	2740		316
	R106	SiO_2 Hydrophobic	0.007	2560		201
	A 300	SiO_2 Hydrophilic	0.007	2560		296
	R972	SiO_2 Hydrophobic	0.016	2560		195
Xu and Zhu [47]		Talc	4.1	2720	No vibration	390
		$CaCo_3$	5.5	2700		230
					With Vibration	247
						190
Guo et al. [71]		SiO_2 Hydrophilic	0.0075	2560	Sound assisted	63
		SiO_2 Hydrophobic	0.0075	2560	at SPL = 100	89
		SiO_2 Hydrophilic	0.50	2560		92
Valverde and Castellanos [118]	R974	SiO_2	0.012	2560		172
	R974	SiO_2	0.012	2560	Magnetic field	172
	R974	SiO_2	0.012	2560	Sound assisted	172
	R974	SiO_2	0.012	2560	Initial vibration	172
	A 300	SiO_2 Hydrophilic	0.007	2200		307
	A 300	SiO_2 Hydrophilic	0.007	2200	Preheating	188
					Centrifugal field	
		TiO_2 Hydrophilic	0.007	4000	$\Lambda = 5$	180
		TiO_2 Hydrophilic	0.007	4000	$\Lambda = 37$	111
		TiO_2 Hydrophilic	0.007	4000	$\Lambda = 82$	93

VII. Applications

Fine particles with their high surface area and unique properties are very attractive for many applications. Control over their size, shape, consistency and composition are necessary and important to ensure their specific commercial applications and to comply with application requirements.

Challenges explained in previous sections limit large-scale application of the nanoparticle fluidized bed. Most applications have only been developed in laboratories or small-scale production.

However, in recent years the production of material with unique specification by nanoparticle fluidization has attracted a lot of attention. The subject is particularly important in food and pharmaceutical industries where drying, cooling, coating, and granulation are frequent applications of a fluidized bed of fine powders.

Using one or more of the assisting methods to obtain homogeneous fluidization of nano-agglomerates can be further processed in large quantities in the dry state using unit operations, such as reaction, coating, granulation, mixing, drying, and adsorption.

One of the most common applications of a nano-particle fluidized bed is coating and encapsulations. Wank et al. [128] carried out Atomic Layer Deposition (ALD) of alumina (Al_2O_3) on a wide size distribution of hexagonal boron nitride platelet-like particles that were fluidized as aggregates in the fluidized bed. They found that the individual primary particles, rather than the aggregates, were coated with a nano-thick ceramic film using ALD.

Cohesive primary particles that fluidized as aggregates in a fluidized bed can be individually coated when the surface reaction is dominant.

Fluidization of nano-agglomerates can also be used for the production of more advanced materials via coating processes.

Esmaeili et al. [129] applied nano-particle fluidization for coating aluminum powders with polymer, which is known as a solution to protect them from a non-desirable reaction, such as oxidation.

Ultrafine alumina powders are being recognized as a good candidate for diverse combustion applications, such as additives in solid rocket propellants and metallic fuel in explosive formulations. The nano-sized aluminum powder showed a burning rate 5-10 times greater than micro-sized ones when used in a gas generator fuel. They can be used to achieve more complete combustions. The enhanced properties are due to their large specific surface area, which provides these powders with a high reactivity and makes them particularly difficult to maintain in an un-oxidized state. Encapsulating nanoparticles with polymers also has applications for medical purposes.

For example, the high mechanical and thermal properties of zirconia had led to its use in applications requiring high temperature, high strength, toughness, and aesthetic shade.

For this reason zirconium oxide has been extensively used in medical and dental applications. To manufacture an artificial denture, zirconia powder on a nanometer scale is densified under high pressure and temperature to obtain a dense ignot, which will be formed to the desired shape via milling by diamond burs. In this process, zirconia powder must be applied on a nanometer scale to avoid anisotropy in the final product. The hard processing of dense sintered zirconia is very time consuming and costly due to wear and tear on the milling instrument.

One possible solution is to encapsulate the zirconia nanoparticles beforehand with a thin layer of polymers, which is uniformly applied around the particles, thus eliminating drawbacks in the milling process [9].

Nanoparticles also have been used to solve environmental issues.

Nishii et al. [130] achieved high-density compacts without the use of a binder to avoid dust formation.

The cohesiveness of fine particles was advantageously exploited in pressure swing granulation to make weakly consolidated agglomerates.

Catalytic gas-solid reaction is another application of the nano-particle fluidized bed.

Klvana et al. [12] developed a new process for hydrogenation of toluene by the use of a Ni/SiO_2 aerogel catalyst, which can yield the high concentration needed in the process.

Matsuda et al. [131] used a fluidized bed of ultrafine particle photo-catalyst for the treatment of NO_x since the amount of NO_x removal is thought to be dependent on the specific surface area of photo-catalyst.

Carbon nanotubes (CNTs) are very promising materials in a wide range of potential applications, e.g., as hydrogen storage media, selective absorption agents, catalyst supports, microelectronic devices, reinforcement materials and so on.

Catalytic chemical vapour deposition (CCVD) in a fluidized bed is one of the successful techniques to synthesize CNTs.

Fluidization is a process of choice for the large scale production of CNTs because such reactors provide a large effective surface area and plenty of space for the growth of CNTs.

In addition, it provides good conditions for rapid heat and mass transfer.

Recently, the production of multi-walled carbon nanotubes (MWNT) using fluidized bed reactors has been of interest to researchers.

Corris et al. [132] employed a fluidized bed reactor for the production of multi-walled carbon nano-tubes with an iron-supported catalyst by the catalytic chemical vapor deposition process.

Multi-walled carbon nano-tubes and single walled carbon nano-tubes are expected to usher in significant breakthroughs in the technology of electronic and engineering materials. The fluidized bed can provide the large-scale synthesis of this material for commercial applications.

Qian et al. [133] also prepared carbon nano-tubes from ethylene decomposition over the Fe/Al_2O_3 catalyst in a so-called nano-agglomerate fluidized bed reactor. Carbon nano-tube with good morphology, narrow diameter distribution and fewer lattice defects were produced.

Large-scale production of carbon nano-tubes with uniform properties will be feasible since the flow dynamic, available space for growing, and the mass and heat transfer rate can be controlled.

VIII. Expansion of the Bed of Fine/Ultrafine Particles

In this section the aim is to determine which of the different forms of the R-Z equation available in the literature is the most appropriate one for predicting the expansion behavior of the bed of fine/ultrafine particles. In this regard, it is of prime importance to be taken into account that the parameters used in the right correlation should reveal the physics of the bed.

Richardson and Zaki [81] developed Eq. (50) to describe the sedimentation and homogeneous fluidization of uniformly sized noncohesive particles ($d_p > 100\mu m$) fluidized with different liquids:

$$\frac{u_{0l}}{u_{p0}} = \varepsilon^n = (1-\emptyset)^n \tag{50}$$

where u_{0l} is the superficial liquid velocity, u_{p0} is the velocity required to give $\varepsilon = 1$ that is theoretically equal to the terminal velocity for an isolated particle, n is the so-called R-Z exponent, and $\emptyset$ is the particle volume fraction. According to Richardson and Zaki [81], sedimentation of suspension and homogeneous fluidization are equivalent processes.

In their experimental work, they observed that the settling velocity of a vertical suspension at a given solid

concentration $u_s(\emptyset)$ was equal to the upward superficial velocity of the liquid required to maintain the fluidized bed at the same solid concentration.

They showed that the parameter n can be correlated to terminal velocity Reynolds number Re_t, based on the diameter and terminal velocity of a single particle, as follows:

$$\begin{gathered} n = 4.65, (Re_t \leq 0.2) \\ n = 4.35\, Re_t^{-0.03}, (0.2 < Re_t \leq 1.0) \\ n = 4.45\, Re_t^{-0.01}, (1.0 < Re_t < 500) \\ n = 2.39, (Re_t \geq 500) \end{gathered} \quad (51)$$

Surprisingly, researchers have found that plotting the homogeneous bed expansion data of fine particles in a gas-solid fluidization system as $\log u_0$ against $\log \varepsilon$ showed the straight line characteristics of liquid-solid systems.

However, the n exponent in Eq. (50), when the superficial gas velocity u_0 instead of u_{0l} was used for gas-solid system, was somewhat larger than predicted for fluidization of uniform spheres with a liquid and u_{p0} was generally greater than the free falling velocity of the particle [134]-[137].

Accordingly, authors tried to relate this phenomenon to the role of interparticle forces for fine cohesive powders since interparticle forces are virtually absent in a liquid fluidized system [134], whereas it is not the case for gas-solid fluidization of fine cohesive particles.

Geldart and Wong [134] studied the expansion characteristics of homogeneous fluidized beds of a wide range of powders having a mean particle size of 3.0 to $125\mu m$ at ambient conditions using various gases, such as air, argon, nitrogen and arction-12.

By using the original R-Z equation for a gas-solid system as given in Eq. (52), they found that the n exponent increased as the particle size decreased and the materials became more cohesive.

In fact, the n exponent was around 4.65 for group A powders and became significantly larger, even as large as 60.0, for those powders, which showed a higher degree of cohesiveness:

$$\frac{u_0}{u_{p0}} = \varepsilon^n = (1-\emptyset)^n \quad (52)$$

Geldart and Wong regarded the values of n/4.65 > 1 as indicative of the presence of interparticle forces in the gas-solid fluidized system.

According to this and on the basis of their experimental results, they correlated the n/4.65 ratio to the Hausner ratio, which itself is a good reflection of the degree of cohesivity of fine particles in the gas-solid system, as follows:

$$\frac{n}{4.65} = \left(\frac{HR}{1.11}\right)^{4.16} \quad (53)$$

Also, they observed that for noncohesive particulate materials, which were uniformly fluidized in a laminar flow regime, the terminal velocity for an isolated particle calculated from the Stokes's equation, u_{p0}, was close to the velocity extrapolated from Eq. (52) at $\varepsilon = 1$, ${u_{p0}}^*$. In contrast, for the cohesive group C particles, the ${u_{p0}}^*/u_{p0}$ was significantly higher than 1.

On the basis of their experimental results, since those materials having n/4.65 > 1 also had a value of ${u_{p0}}^*/u_{p0} > 1$, they correlated these two ratios as follows:

$$\frac{n}{4.65} = 1.26\left(\frac{{u_{p0}}^*}{u_{p0}}\right)^{0.132} \quad (54)$$

According to what was proposed by Geldart and Wong [134], to predict the homogeneous bed expansion behavior of fine cohesive particles in a gas-solid fluidized bed using Eq. (52), the value of n index can be predicted from Eq. (53) by having the value of the Hausner ratio for the powder, and ${u_{p0}}^*/u_{p0}$ from n through Eq. (54), while u_{p0} is calculated from Stokes's equation using the mean particle size.

As can be found from this strategy, the accuracy of the prediction is highly dependent on the experimentally determined value of the Hausner ratio.

However, although Geldart and Wong [134] showed that this method can have acceptable results for micron size fine particles, the applicability of this method for prediction of the uniform bed expansion behavior of nanoparticles is highly questionable because, as noted by Esmaeili et al. [9], the Hausner ratio is not a good indication of the fluidization behavior of nano size particles.

Next, and more importantly, although the value of n index in this strategy is reflective of the cohesiveness inside the bed and increases by increasing the bed cohesivity, this form of R-Z equation is not a good phenomenological representation of the bed expansion behavior of fluidizing entities inside the bed of fine/ultrafine powders.

As previously stated, fine/ultrafine primary particles tend to cross the fluidizability barrier by forming agglomerates of the primary powders.

When these agglomerates uniformly expand in their stable fluidization regime, hydrodynamic forces are dominant forces in this gas-solid system [19] and, hence, having a form of R-Z equation with a value of n exponent near 5.0 in laminar flow regime, as noted by Geldart and Wong [134], would be a better choice for this case in which interparticle forces are fairly absent between fluidizing entities.

In this form, the value of n index, $n \cong 5.0$, phenomenologically represents the physics of agglomerate fluidization of fine/ultrafine particles, when they smoothly expand in the bed.

To confirm this fact, it was noted by Zhu et al. [1] that

the Reynolds number for APF nanoparticle agglomerates, which can fluidize uniformly without any bubbles, is typically very small (Re < 1) and, hence, Stokes flow prevails for them.

Therefore, the R-Z exponent cannot deviate too much from $n \approx 5$ [1].

Also, it was shown by Nam et al. [32] that a R-Z exponent of n = 5.0 is valid for APF nanoparticle aggregates.

In order to have a form of R-Z equation that describes well the physics of agglomerate fluidization of fine/ultrafine particles, it is necessary to make two more modifications to Eq. (52).

First, since agglomerates of primary particles are fluidizing entities in a gas-solid fluidized bed of fine/ultrafine particles, substituting the u_{p0} by the terminal velocity of the agglomerates u_{tsa} is required. Second, again, due to the preceding stated reason and noting the fact that these agglomerates have fractal structures, which effectively screen the gas flow as gas flow inside the aggregates is negligible compared to the flow outside [123], it requires the use of agglomerate concentration $\emptyset_a$ rather than solid concentration in Eq. (52).

All points discussed here direct us to the modified Richardson-Zaki equation coupled with fractal analysis proposed by Valverde et al. [115], Castellanos et al. [41], and Nam et al. [32], which is expressed as follows:

$$\frac{u_0}{u_{tsa}} = (1 - \emptyset_a)^{5.0} \tag{55}$$

or by using the concept of fractal analysis, which was explained in section 6.3, it can be given in a more complete form as the following:

$$\frac{u_0}{\frac{N_a}{k_a}\, u_{p0}} = \left(1 - \emptyset \frac{{k_a}^3}{N_a}\right)^{5.0} \tag{56}$$

It is stressed here that Eq. (55) or (56) is the most appropriate form of R-Z equation for prediction of the bed expansion behavior of agglomerate fluidization of fine/ultrafine particles, which each of its components phenomenologically describes the physics behind the fluidization of these materials.

It is worth recalling here that for the other forms of R-Z equation, which were proposed by Yao et al. [20], Eq. (39), only replaces the particle falling velocity by the agglomerate settling velocity in Eq. (52) and, hence, doesn't consider all required modifications that should be done on Eq. (52) for agglomerate fluidization of fine/ultrafine powders.

The inability of this form for prediction of bed expansion behavior of agglomerate fluidization of ultrafine particles can be found in the experimental results of Yao et al. [20] where the predicted values of n exponent for beds of APF agglomerates for which, as noted above, the Reynolds number is very low and laminar flow condition is dominating, were as low as 3, which is typically close to the values of n reported for the turbulent regime of liquid-solid fluidization of non-agglomerated particles [81].

Even though it is expressed that Eq. (56) is much better than the form of R-Z equation proposed by Geldart and Wong [134], which based on their experimental observations can be given as the following:

$$\frac{u_0}{{u_{p0}}^*} = \frac{u_0}{u_{tsa}} = (1 - \emptyset)^n \tag{57}$$

Eq. (57) was very effective in determining the degree of importance of interparticle forces in beds of micron size fine particles by merely evaluating the magnitude of n index from their uniform bed expansion data. Therefore, it is highly interesting to check whether Eq. (57) keeps its predictive ability for reflecting the degree of cohesivity by values of n exponent in beds of other fine/ultrafine materials, especially nanoparticles, that have been used by different researchers to verify Eq. (56) or not.

Frankly speaking, the left hand sides of both Eqs. (56) and (57) for a specific bed of fine/ultrafine particulate bed with a specific agglomerate size are equivalent because both indicate that agglomerates of the primary particles are fluidizing entities in the system and, hence, the terminal velocity of agglomerate is used in both correlations.

Therefore, in order to calculate the value of n exponent in Eq. (57) from the bed expansion data attainable from Eq. (56), the right hand side of these two correlations should be equivalent, too.

By doing so, the mean values of n exponent for different solid systems, in their own homogeneous bed expansion regime, are calculated and presented in Table V.

As can be found in Table V, similar to what was reported by Geldart and Wong [134], Eq. (57) predicts values of n larger than 4.65 for gas-solid systems of micron size fine particles.

The most striking result is found for the system of nanoparticle for which $n = 350$ is calculated.

As expected, the magnitude of interparticle force for a bed of nano size particle is much greater than the bed of the same type of material but with larger size particles and this can be clearly found from the value of n index reported for this size of powder in Table V.

Albeit this verification was done for one nanoparticle material here, performing the same type of calculations by having the bed expansion data for other nano size powders seems necessary to confirm the ability of Eq. (57) for predicting the importance of interparticle forces in a gas-solid system of ultrafine particles by merely providing the homogeneous bed expansion data of the system.

TABLE V
CALCULATION OF n EXPONENT OF EQ. (57) FOR FINE/ULTRAFINE POWDERS USED BY DIFFERENT RESEARCHERS TO VERIFY EQ. (56)

Source	Material	d_p (μm)	ρ_p (kg/m^3)	N_a	D	Calculated n for Eq. (57)
Valverede et al. [115]	Xerographic toner	8.53	1199	96	2.6190	11.17
Castellanos et al. [41]	Copolymer styrene n-buthylmethacyrylate	7.8	1135	63	2.5323	12.70
		11.8		23.7	2.5120	10.51
		15.4		12.4	2.4990	9.42
		19.1		9.6	2.5080	8.64
Nam et al. [32]	Aerosil R974	0.012	2200	4.047×10^{10}	2.5371	350.22

IX. Future Work

Research on the concept of fluidization of fine/ultrafine particles has been conducted over the last three decades. However, although many valuable studies have been carried out, there is not a well-matured knowledge in the field and, hence, fine cohesive powders, including ultrafine or nano size powders, play a moderate role in industrial applications nowadays. Nonetheless, it is highly expected that theses powders will be significantly important in industrial applications in the near future due to their special characteristics, namely their very small primary size and large surface area-to-volume ratio. Therefore, much more scientific efforts are required to expand the knowledge for ultrafine particle fluidization in order to facilitate the implementation of large scale industrial processes involving these materials.

First and foremost, introducing a simple and robust criterion for predicting APF/ABF behavior of ultrafine powders or modifying the existing ones seems essential. As discussed before, the one which was proposed by Yao et al. [20] and Zhu et al. [1] is simple and only requires the primary particle size and bulk density. However, even though it could have acceptable results for different nanoparticle samples, it is not robust enough for the purpose. On the other hand, the other criterion, which was proposed by Romero and Johanson [61], has very good sensitivity to APF and ABF behaviors as long as there is a good evaluation of the minimum fluidization velocity of the powders, which itself is a challenging task for such fine and ultrafine cohesive particles. Another problem with this criterion is that it was only verified for some nano size particles. Thus, performing more studies seems essential to check whether this classification criterion is applicable for all nanopowders or not.

Second, it was noted in previous sections that effective fluidization of fine/ultrafine cohesive particles is often not possible without an assisting method; different groups of researchers showed that the fluidization quality of these powders could, however, be greatly enhanced when an appropriate assisting method was applied. Apart from all the research work that has been performed in this part, there are still many holes remaining to be filled in order to understand better the exact performance of each technique. Improving the fluidization quality of fine/ultrafine particles with the combination of the proposed methods is the matter, which has received little attention among researchers, whereas this might be a helpful solution for increasing the efficiency of assisting approaches. Furthermore, coming up with novel assisting methods demanding low energy and cost, that are easy to implement and scale up together with considerable efficiency in practice is highly appreciated.

Third, the mean agglomerate size is an important parameter to be evaluated, when a bed of ultrafine powders is fluidizing, due to its substantial impact on the quality of fluidization, the heat and mass transfer efficiencies and on the overall performance of the fluidized bed. In this regard, considerable efforts have been devoted to measure and predict this parameter. Concerning the online measurement of the agglomerate size, it seems that the X-ray imaging technique is a powerful one, which can provide researchers with plenty of structural and dynamic information about the fluidized bed of ultrafine particles in a noninvasive manner. However, further development is required for the technique to respond to the low X-ray energies needed for some fine powder samples. In parallel and most necessarily, more studies are required to present a simple model for predicting the agglomerate size from some preliminary information, including the physical properties of the particulate material, interparticle attractive forces, and operating parameters independent of the introduction of many fitting parameters to be assumed. The simple model proposed by Valverde and Castellanos [118] would be a sample for such modeling. Nonetheless, it predicts the same agglomerate size for non-assisted, sound-assisted, magnetically-assisted fluidized beds and also for the bed assisted by mechanical vibration, whereas, according to the experimental results reported by different researchers that cannot be the case. In addition, it is of great importance to experimentally verify whether the superficial gas velocity affects the mean agglomerate size or not. If it does, it is highly appreciated to be considered when models will be presented for estimating agglomerate size. This is the case when an agreement among the research community does not exist and it needs to be well clarified with the help of experimental results.

As suggested by van Ommen and Pfeffer [4], another virtually unexplored field is the modeling of reactions taking place in a fluidized bed of ultrafine particles. Considering the fact that one agglomerate of ultrafine particles can easily consist of too many primary particles, a large range of length scales plays a role in this modeling and, hence, a multi-scale modeling approach would be an appropriate one for this purpose [4].

One of the critical applications of the nanoparticle fluidized bed is for encapsulation of nanoparticles. Coating or encapsulating nanoparticles with polymers is desired in many applications to improve their chemical stability, reduce their toxicity, and facilitate their storage, transport, and processing. In two particular applications of nanoparticle coating, we can specify the encapsulation of zirconia and aluminum nanoparticles. These nanoparticles are very promising materials in industrial applications. Over the last few years, the introduction of zirconium oxide-based ceramics into the field of dentistry has been greatly appreciated. On the other hand, ultrafine aluminum powder is being recognized as a good candidate for diverse combustion applications, such as additives in solid rocket propellants and metallic fuel in explosive formulations. The common method for encapsulation of nanoparticles is slurry based methods in which small amounts of catalyst is dissolved in an organic solvent, where nanoparticles have already been dispersed. Some drawbacks, however, arise when the process is carried out in the liquid phase, as the polymerization reaction must be followed by additional steps to isolate the coated particles. After encapsulation, the reaction slurry must be filtered to separate the coated particles from the solvent. This step is usually accompanied by washing the encapsulated powders to eliminate solvent impurities, catalyst and the nonreacted monomers. Then, the coated particles must be completely dried in an oven overnight. Subsequently, the dried particles form a hard bulk material, which needs to be grinded to obtain finely coated particles. To accomplish all of the aforementioned additional processes requires more than the polymerization reaction time itself, which usually lasts only a few minutes. Accordingly, the encapsulation process costs for a liquid–solid reaction, particularly when dealing with large amounts of particles, are significant. In addition, under these conditions, it is difficult to ensure a complete removal of the impurities in the solvent and to obtain the desired particle size by grinding the bulk material recovered from the process. To overcome these issues Esmaeili et al. [129] for the first time used a fluidized bed reactor for encapsulating nanoparticles by the polymerization compounding approach using Ziegler–Natta catalysts. The polymerization reaction was carried out using a solvent-free process in a gas-solid fluidized bed reactor. This direct gas–solid reaction greatly simplified collecting the particles of interest after polymerization because there was none of the extra steps often found in encapsulation processes, such as filtering and drying. Although the concept has been approved on a lab scale, scaling up of such a process still is a big challenge. It is necessary to evaluate fluidization quality on a large scale and define proper operating conditions to be able to encapsulate nanoparticles at that scale. In parallel, more studies relating to the coating of ultrafine particles with a thin layer of organic and/or inorganic materials to achieve a specific physical, chemical, optical, and electrical property are required to be performed. All of these studies should be directed to the ideal conditions of coating the individual nanoparticles, rather than their agglomerates, in the simplest practical way.

X. Summary

Ultrafine powders, nanoparticles, have received widespread interest in recent years due to their unique properties arising from their very small primary particle size and very large surface area. They have been used to produce catalysts, effective sorbents, drugs, cosmetics, food and plastics. In addition, they have some applications in hydrogen storage, Li-ion batteries, and fuel cells. In parallel with plenty of academic attention on the fluidization of nanoparticles, it is a highly probable that these powders will be incorporated as part of large-scale industrial processes. Accordingly, it will require large quantities of ultrafine particles to be handled and processed in many cases. Prior to processing such materials, however, it is necessary that the nano-sized particles be well dispersed. Gas fluidization is one of the best techniques available to disperse and process fine particles. Gas-solid fluidized beds are among the unit operations, which have a number of significant advantages for processing small solid particles, including high heat and mass transfer rates, uniform and controllable bed temperature, the ability to handle a wide variety of particle properties and suitability for large-scale operations. Since the fluidization of nanoparticles happens in an agglomerate state, the properties of fluidized agglomerates, rather than those of primary powders, determine the fluidization characteristics of the bed. Thus, it is very important to know how these aggregate particles fluidize within the bed. Fluidization of nanoparticle agglomerates suffers from several problems, such as bubbling, channeling, clustering, and entrainment. Therefore, inappropriate dispersion of nanoparticles in the gas phase and considerable gas bypassing may occur. Moreover, for the conventional gravity-driven fluidization of nanoparticles, even in particulate fluidization, appreciable powder elutriation happens at the high superficial gas velocities required to fluidize the nano-aggregates. This loss of particles is probably the main reason that prevents the application of gas fluidization of nano-agglomerates in industrial processes. To overcome these problems and improve the fluidization quality of nanoparticle agglomerates, various assisting methods have been proposed and tested. These methods include vibration, ultra-sound, the application of magnetic and electric fields, the use of a rotating fluidized bed, the use of a conical fluidized bed, the addition of foreign particles and the use of micro-jets as a secondary flow in the bed. The degree of fluidization enhancement achieved by applying these methods is evaluated by measuring some hydrodynamic parameters, such as minimum fluidization velocity, bed pressure drop, bed expansion, agglomerate size, degree of mixing, bubble suppression and amount of powder elutriation, as indicators of fluidization quality.

This review intended to provide a comprehensive review of current ultra fine powder fluidization technology. It discussed the challenges associated with widespread application of these powders in industries and explained the fundamentals of nanoparticle fluidization along with the details necessary to understand the process complexity and come up with reliable solutions. It gives in-depth coverage of state-of-the-art international research experiences of nanoparticle fluidization at the edge of scientific inquiry and emerging technologies.

Fluidization of the nanoparticle is state of the art. Engineers and scientists in the chemical and pharmaceutical fields as well as in the areas of agriculture, food, ceramics, electronics and solid-catalyzed reactions need to broaden their current level of knowledge. The engineering data available for its implementation are limited and this subject requires more research. More studies are necessary to describe how the assisting method can improve the quality of fluidization and how operating parameters can be adjusted to achieve desirable homogeneity. It can be suggested to perform different tests at a wide range of vibration (f=0-50 Hz) and monitor bubble formation at different vibration intensities. Size and propagation also can be studied. Enhancing nano-fluidization with an electrostatic field also needs extensive studies. This can be done for a variety of nanoparticles at different electrostatic fields. Pre-charging powders prior to fluidization could also be considered as an alternative subject or other design parameters, like distributer geometry, the effect of internals, and heat and mass transfer, could attract the researcher's attention to fill the holes in the body of knowledge.

References

[1] C. Zhu, Q. Yu, R. N. Dave, R. Pfeffer, Gas fluidization characteristics of nanoparticle agglomerates, *AIChE J.* 51 *(2005)* 426-439.

[2] J. Quevedo, R. Pfeffer, Y. Shen, R. Dave, H. Nakamura, S. Watano, Fluidization of nanoagglomerates in a rotating fluidized bed, *AIChE J. 52* (2006) 2401-2412.

[3] E. Jaraiz, S. Kimura, O. Levenspiel, Vibrating beds of fine particles: Estimation of interparticle forces from expansion and pressure drop experiments, *Powder Technol. 72* (1992) 23-30.

[4] J. R. van Ommen, R. Pfeffer. Fluidization of Nanopowders-Experiments, Modeling, and Applications, *13th International Conference on Fluidization,* Gyeong-ju, Korea, 16-21 May (2010).

[5] J. R. van Ommen, D. M. King, A. Weimer, R. Pfeffer, B. G. M. van Wachem, Experiments and modelling of micro-jet assisted fluidization of nanoparticles, *13th International Conference on Fluidization,* Gyeong-ju, Korea, 16-21 May (2010).

[6] D. Kunii, O. Levenspiel, *Fluidization Engineering* (Butterworth-Heinemann, 1991).

[7] G. H. Qian, I. Bágyi, I. W. Burdick, R. Pfeffer, H. Shaw, J. G. Stevens, Gas–solid fluidization in a centrifugal field, *AIChE J. 47* (2001) 1022-1034.

[8] S. Sanaei, N. Mostoufi, R. Radmanesh, R. Sotudeh-Gharebagh, C. Guy, J. Chaouki, Hydrodynamic characteristics of gas–solid fluidization at high temperature, *Can. J. Chem. Eng. 88* (2010) 1-11.

[9] B. Esmaeili, J. Chaouki, C. Dubois, An evaluation of the solid hold-up distribution in a fluidized bed of nanoparticles using radioactive densitometry and fibre optics, *Can. J. Chem. Eng. 86* (2008) 543-552.

[10] D. Geldart, Types of gas fluidization, *Powder Technol. 7* (1973) 285-292.

[11] P. Ammendola, R. Chirone, F. Raganati, Fluidization of binary mixtures of nanoparticles under the effect of acoustic fields, *Adv. Powder Technol. 22* (2011) 174-183.

[12] D. Klvana, J. Chaouki, C. Lauga, C. Chavarie, D. Kusohorsky, G. Pajonk, Study of the performance of fluidization Ni/SiO2 aerogel for toluene hydrogenation, *6th International Conference on Fluidization,* Banff, Canada (1989).

[13] J. Visser, Van der Waals and other cohesive forces affecting powder fluidization, *Powder Technol.* 58 *(1989) 1-10.*

[14] A. Dutta, L. V. Dullea, Effects of external vibration and the addition of fibers on the fluidization of a fine powder, *AIChE Sym. Ser. 87* (1991) 38–46.

[15] J. Chaouki, C. Chavarie, D. Klvana, G. Pajonk, Effect of interparticle forces on the hydrodynamic behaviour of fluidized aerogels, *Powder Technol. 43* (1985) 117-125.

[16] Chavarie C., K. Dobson, R. Clift, J. P. K. Seville, Study on the fluidization of group C aerogel powders by spontaneous dynamic agglomeration, *37th Canadian Chemical Engineering Conference,* Montreal, Canada (1987).

[17] S. Morooka, K. Kusakabe, A. Kobata, Y. Kato, Fluidization state of ultrafine powders, *J. Chem. Eng. J. 21* (1988) 41–46.

[18] A. W. Pacek, A. W. Nienow, Fluidisation of fine and very dense hardmetal powders, *Powder Technol. 60* (1990) 145-158.

[19] Y. Wang, F. Wei, Y. Jin, T. Luo, Agglomerate particulate fluidization and E-particles, *Third Joint China/USA Chemical Engineering Conference (CUChE-3)*, Beijing, China (2000).

[20] W. Yao, G. Guangsheng, W. Fei, W. Jun, Fluidization and agglomerate structure of SiO2 nanoparticles, *Powder Technol. 124* (2002) 152-159.

[21] L. F. Hakim, J. L. Portman, M. D. Casper, A. W. Weimer, Aggregation behavior of nanoparticles in fluidized beds, *Powder Technol. 160* (2005) 149-160.

[22] J. A. Quevedo, A. Omosebi, R. Pfeffer, Fluidization enhancement of agglomerates of metal oxide nanopowders by microjets, *AIChE J. 56* (2010) 1456-1468.

[23] C. Zhu, G. Liu, Q. Yu, R. Pfeffer, R. N. Dave and C. H. Nam, Sound assisted fluidization of nanoparticle agglomerates, *Powder Technol. 141* (2004) 119-123.

[24] H. Liu, Q. Guo, S. Chen, Sound-Assisted Fluidization of SiO2 Nanoparticles with Different Surface Properties, *Ind. Eng. Chem. Res. 46* (2007) 1345-1349.

[25] P. Ammendola, R. Chirone, F. Raganati, Sound assisted fluidization of Al2O3and Fe2O3 nanoparticles, *AIChE Annual Meeting,* Salt Lake City, US, November 7-12 (2010).

[26] P. Ammendola, R. Chirone, Aeration and mixing behaviours of nano-sized powders under sound vibration, *Powder Technol. 201* (2010) 49-56.

[27] S. Kaliyaperumal, S. Barghi, J. Zhu, L. Briens and S. Rohani, Effects of acoustic vibration on nano and sub-micron powders fluidization, *Powder Technol. 210* (2011) 143-149.

[28] J. M. Valverde, M. J. Espin, M. A. S. Quintanilla, A. Castellanos, Electrofluidized bed of silica nanoparticles, *J. Electrostatics 67 (2009) 439-444.*

[29] D. Lepek, J. M. Valverde, R. Pfeffer, R. N. Dave, Enhanced nanofluidization by alternating electric fields, *AIChE J. 56 (*2010) 54-65.

[30] Q. Yu, R. N. Dave, C. Zhu, J. A. Quevedo, R. Pfeffer, Enhanced fluidization of nanoparticles in an oscillating magnetic field, *AIChE J. 51* (2005) 1971-1979.

[31] P. Zeng, T. Zhou, J. Yang, Behavior of mixtures of nano-particles in magnetically assisted fluidized bed, *Chem. Eng. Process. 47* (2008) 101-108.

[32] C. H. Nam, R. Pfeffer, R. N. Dave, S. Sundaresan, Aerated vibrofluidization of silica nanoparticles, *AIChE J. 50* (2004) 1776-1785.

[33] J. Yang, T. Zhou, L. Song, Agglomerating vibro-fluidization behavior of nano-particles, *Adv. Powder Technol. 20* (2009) 158-163.

[34] S. Matsuda, H. Hatano, T. Muramoto, A. Tsutsumi, Modeling for size reduction of agglomerates in nanoparticle fluidization,

AIChE J. 50 (2004) 2763-2771.
[35] H. Nakamura, S. Watano, Fundamental particle fluidization behavior and handling of nano-particles in a rotating fluidized bed, *Powder Technol. 183* (2008) 324-332.
[36] R. D. Venkatesh, J. Chaouki, D. Klvana, Fluidization of cryogels in a conical column, *Powder Technol. 89* (1996) 179-186.
[37] C. Brereton, J. Chaouki, J. R. Grace, R. Legros, J. Yeung, Hydrodynamic behavior of a silica aerogel powder in a circulating fluidized bed, *37th Canadian Chemical Engineering Conference,* Montreal, Canada (1987).
[38] C. Lauga, J. Chaouki, D. Klvana, C. Chavarie, Improvement of the fluidisability of Ni/SiO2 aerogels by reducing interparticle forces, *Powder Technol. 65* (1991) 461-468.
[39] L. S. Fan, C. Zhu, *Principles of Gas–Solid Flows* (Cambridge University Press, 1998).
[40] L. G. Gibilaro, *Fluidization Dynamics* (Butterworth Heinemann, 2001).
[41] A. Castellanos, J. M. Valverde, M. A. S. Quintanilla, Aggregation and sedimentation in gas-fluidized beds of cohesive powders, *Phys. Rev. E 64* (2001) 041304.
[42] F. London, The general theory of molecular forces, *Trans. Faraday Soc. 33* (1937) 8-26.
[43] H. Krupp, Particle Adhesion: Theory and Experiment, *Adv. Colloid Interface Sci. 1* (1967) 111.
[44] O. Molerus, Interpretation of Geldart's type A, B, C and D powders by taking into account interparticle cohesion forces, *Powder Technol. 33* (1982) 81-87.
[45] L. Massimilla, G. Donsì, Cohesive forces between particles of fluid-bed catalysts, *Powder Technol. 15* (1976) 253-260.
[46] T. G. Mason, A. J. Levine, D. Ertascedil, T. C. Halsey, Critical angle of wet sandpiles, *Phys. Rev. E 60* (1999) R5044.
[47] C. Xu, J. Zhu, Experimental and theoretical study on the agglomeration arising from fluidization of cohesive particles--effects of mechanical vibration, *Chem. Eng. Sci. 60* (2005) 6529-6541.
[48] J. M. Valverde, A. Ramos, A. Castellanos, P. Keith Watson, The tensile strength of cohesive powders and its relationship to consolidation, free volume and cohesivity, *Powder Technol. 97* (1998) 237-245.
[49] J. P. K. Seville, C. D. Willett, P. C. Knight, Interparticle forces in fluidisation: a review, *Powder Technol. 113* (2000) 261-268.
[50] A. G. Bailey, Electrostatic phenomena during powder handling, *Powder Technol. 37* (1984) 71-85.
[51] K. Rietema, *The Dynamics of Fine Powders* (Elsevier Science Publishers LTD, 1991).
[52] G. Lian, C. Thornton, M. J. Adams, A Theoretical Study of the Liquid Bridge Forces between Two Rigid Spherical Bodies, *J. Colloid Interface Sci. 161* (1993) 138-147.
[53] T. Weigert, S. Ripperger, Calculation of the Liquid Bridge Volume and Bulk Saturation from the Half-filling Angle, *Part. Part. Syst. Charact. 16* (1999) 238-242.
[54] O. Gundogdu, U. Tuzun, Gas Fluidisation of Nanoparticle Assemblies: Modified Geldart classification to account for multiplescale fluidisation of agglomerates and clusters, *KONA 24* (2006) 3-14.
[55] Z. Wang, M. Kwauk, H. Li, Fluidization of fine particles, *Chem. Eng. Sci. 53* (1998) 377-395.
[56] H. Cui, J. Chaouki, Interparticle forces in high temperature fluidization of geldart a particles, *China Particuology 2* (2004) 113-118.
[57] J. P. K. Seville, R. Clift, The effect of thin liquid layers on fluidisation characteristics, *Powder Technol.* 37 (1984) 117-129.
[58] M. J. Rhodes, X. S. Wang, A. J. Forsyth, K. S. Gan, S. Phadtajaphan, Use of a magnetic fluidized bed in studying Geldart Group B to A transition, *Chem. Eng. Sci. 56* (2001) 5429-5436.
[59] J. Shabanian, F. Fotovat, J. Bouffard, J. Chaouki, Fluidization Behavior in a Gas-Solid Fluidized Bed with Thermally Induced Inter-particle Forces, *10th International Conference On Circulating Fluidized Beds And Fluidization Technology- CFB-10, Engineering Conferences International.* Sunriver Resort, Oregon, US, May 1-5, (2011).
[60] D. Geldart, N. Harnby, A. C. Wong, Fluidization of cohesive powders, *Powder Technol. 37* (1984) 25-37.
[61] J. B. Romero, L. N. Johanson, Factors affecting fluidized bed quality, *Chem. Eng. Prog. Sym. Ser. 58* (1958) 28-37.
[62] W. C. Yang, Fluidization of fine cohesive powders and nanoparticles-a review, *J. Chin. Inst. Chem. Eng. 36* (2005) 1–15.
[63] Q. Guo, Y. Li, M. Wang, W. Shen, C. Yang, Fluidization Characteristics of SiO2 Nanoparticles in an Acoustic Fluidized, *Chem. Eng. Technol. 29* (2006) 78-86.
[64] R. D. Morse, Sonic Energy in Granular Solid Fluidization, *Ind. Eng. Chem. Res. 47* (1955) 1170-1175.
[65] R. Chirone, L. Massimilla, S. Russo, Bubbling fluidization of a cohesive powder in an acoustic field, *Fluidization VII* (1992) 545–553.
[66] R. Chirone, L. Massimilla, S. Russo, Bubble-free fluidization of a cohesive powder in an acoustic field, *Chem. Eng. Sci. 48* (1993) 41-52.
[67] P. Russo, R. Chirone, L. Massimilla, S. Russo, The influence of the frequency of acoustic waves on sound-assisted fluidization of beds of fine particles, *Powder Technol. 82* (1995) 219-230.
[68] E. K. Levy, I. Shnitzer, T. Masaki, J. Salmento, Effect of an acoustic field on bubbling in a gas fluidized bed, *Powder Technol. 90* (1997) 53-57.
[69] Q. Guo, H. Liu, W. Shen, X. Yan, R. Jia, Influence of sound wave characteristics on fluidization behaviors of ultrafine particles, *Chem. Eng. J. 119* (2006) 1-9.
[70] Q. Guo, M. Wang, Y. Li and C. Yang, Fluidization of Ultrafine Particles in a Bubbling Fluidized Bed with Sound Assistance, *Chem. Eng. Technol. 28* (2005) 1117-1124.
[71] Q. Guo, X. Yang, W. Shen and H. Liu, Agglomerate size in an acoustic fluidized bed with sound assistance, *Chem. Eng. Process. 46* (2007) 307-313.
[72] S. Mori, A. Yamamoto, S. Iwata, T. Harahan, I. Yamada, Vibro-fluidization of Group C particles and its industrial applications, *AIChE Sym. Ser. 86* (1990) 88–94.
[73] E. Marring, A. C. Hoffmann, L. P. B. M. Janssen, The effect of vibration on the fluidization behaviour of some cohesive powders, *Powder Technol. 79* (1994) 1-10.
[74] K. Noda, Y. Mawatari, S. Uchida, Flow patterns of fine particles in a vibrated fluidized bed under atmospheric or reduced pressure, *Powder Technol. 99* (1998) 11-14.
[75] J. R. Wank, S. M. George, A. W. Weimer, Vibro-fluidization of fine boron nitride powder at low pressure, *Powder Technol. 121* (2001) 195-204.
[76] Y. Mawatari, T. Koide, Y. Tatemoto, S. Uchida, K. Noda, Effect of particle diameter on fluidization under vibration*, Powder Technol. 123* (2002) 69-74.
[77] C. Xu, Y. Cheng, J. Zhu, Fine particle fluidization-effects of mechanical/acoustic vibration, *Fluidization XI,* (2004) 627–634.
[78] J. M. Valverde, A. Castellanos, Effect of vibration on agglomerate particulate fluidization, *AIChE J. 52* (2006) 1705-1714.
[79] W. Zhang, M. Zhao, Fluidisation behaviour of silica nanoparticles under horizontal vibration, *J. Exp. Nanosci. 5* (2010) 69-82.
[80] A. T. Harris, On the vibration assisted fluidisation of silica nanoparticles, *Int. J. Nanotechnol. 5* (2008) 179-194.
[81] J. F. Richardson, W. N. Zaki, Sedimentation and fluidization. Part 1., *Trans. Inst. Chem. Eng. 32* (1954) 35-52.
[82] H. Wang, T. Zhou, J. S. Yang, J. J. Wang, H. Kage, Y. Mawatari, Model for Calculation of Agglomerate Sizes of Nanoparticles in a Vibro-fluidized Bed, *Chem. Eng. Technol. 33* (2010) 388-394.
[83] S. Kaliyaperumal, S. Barghi, L. Briens, S. Rohani, J. Zhu, Fluidization of nano and sub-micron powders using mechanical vibration, *Particuology 9* (2011) 279-287.
[84] S. M. Tasirin, N. Anuar, Fluidization Behavior of Vibrated and Aerated Beds of Starch Powders, *J. Chem. Eng. J. 34* (2001) 1251-1258.
[85] E. K. Levy, B. Celeste, Combined effects of mechanical and acoustic vibrations on fluidization of cohesive powders, *Powder Technol. 163* (2006) 41-50.
[86] K. Erdész, A. S. Mujumdar, Hydrodynamic aspects of conventional and vibrofluidized beds--a comparative evaluation, *Powder Technol. 46* (1986) 167-172.

[87] J. Arnaldos, J. Casal, A. Lucas, L. Puigjaner, Magnetically stabilized fluidization: modelling and application to mixtures, *Powder Technol. 44* (1985) 57-62.
[88] Q. S. Zhu, H.Z. Li, Fluidization of group C powder with external magnetic force, *Fifth China-Japan Symposium on Fluidization,* Nagoya, Japan (1994).
[89] Q. Zhu, H. Li, Study on magnetic fluidization of group C powders, *Powder Technol. 86* (1996) 179-185.
[90] W. Y. Wu, A. Navada, S. C. Saxena, Hydrodynamic characteristics of a magnetically stabilized air fluidized bed of an admixture of magnetic and non-magnetic particles, *Powder Technol. 90* (1997) 39-46.
[91] V. L. Ganzha, S. C. Saxena, Heat-transfer characteristics of magnetofluidized beds of pure and admixtures of magnetic and nonmagnetic particles, *IJHMT 41* (1998) 209-218.
[92] X. Lu, H. Li, Fluidization of CaCO3 and Fe2O3 particle mixtures in a transverse rotating magnetic field, *Powder Technol. 10* (2000) 66-78.
[93] J. A. Quevedo, J. Flesch, R. Pfeffer, R. Dave, Evaluation of assisting methods on fluidization of hydrophilic nanoagglomerates by monitoring moisture in the gas phase, *Chem. Eng. Sci. 62* (2007) 2608-2622.
[94] P. Zeng, T. Zhou, G. Chen, Q. Zhu, Behavior of mixed ZnO and SiO2 nano-particles in magnetic field assisted fluidization, *China Particuology 5* (2007) 169-173.
[95] Zhou L., R. Diao, T. Zhou, H. Wang, H. Kage, Y. Mawatari, Behavior of magnetic Fe3O4 nano-particles in magnetically assisted gas-fluidized beds, *Adv. Powder Technol. 22* (2011) 427-432.
[96] M. Kashyap, D. Gidaspow, T. W. Tsai, Effect of electric field on the hydrodynamics of nanoparticles in a rectangular fluidized bed, *AIChE Annual Meeting,* San Francisco, CA, US, (2006).
[97] M. Kashyap, D. Gidaspow, M. Driscoll, Effect of electric field on the hydrodynamics of fluidized nanoparticles, *Powder Technol. 183 (2008) 441-453.*
[98] J. M. Valverde, M. A. S. Quintanilla, M. J. Espin, A. Castellanos, Nanofluidization electrostatics, *Phys. Rev. E 77* (2008) 031301.
[99] M. A. S. Quintanilla, J. M. Valverde, A. Castellanos, D. Lepek, R. Pfeffer, R. N. Dave, Nanofluidization as affected by vibration and electrostatic fields, *Chem. Eng. Sci. 63* (2008) 5559-5569.
[100] M. A. Howley, R. Pfeffer. The hydrodynamics of a rotating fluidized bed, *AIChE Annual Meeting,* Cicinati, Ohio, US, October 30 - November 04 (2005).
[101] G. H. Qian, R. Pfeffer, H. Shaw, J. Stevens, Fluidization of group C particles using rotating fluidized beds, *Fluidization X* Engineering Foundation*,* (2001) 509-516.
[102] S. Matsuda, H. Hatano, K. Tsuchiya, Effects of Operating Conditions on Photocatalytic Reduction of NOx in Fluidized Beds of TiO2, *Fluidization IX,* Engineering Foundation, (1998) 701-708.
[103] E. K. Levy, W. J. Shakespears, A. T. Raissi, J. C. Chen, Particle elutriation from centrifugal fluidized beds, *AIChE Symp. Ser.* (1981) 86–95.
[104] S. Matsuda, H. Hatano, T. Nuramoto, A. Tsutsumi, Particle and Bubble Behavior in Ultrafine Particle Fluidization with High G, *Fluidization X,* Engineering Foundation*,* (2001) 501–508.
[105] C. Y. Wen, Y. H. Yu, Mechanics of fluidization, *Chem. Eng. Prog. Symp. Ser. 62* (1966) 100-111.
[106] H. Tong, O. Qiu, H. Li, Fluidization Characteristics of Ultrafine Particles in Conical Bed, *Fluidization IX,* Engineering Foundation, (2004) 715-722.
[107] A. Ajbar, Y. Bakhbakhi, S. Ali, M. Asif, Fluidization of nano-powders: Effect of sound vibration and pre-mixing with group A particles, *Powder Technol. 206 (2011) 327-337.*
[108] T. Zhou, H. Li, Effects of adding different size particles on fluidization of cohesive particles, *Powder Technol. 102* (1999) 215-220.
[109] L. Song, T. Zhou, J. Yang, Fluidization behavior of nano-particles by adding coarse particles, *Adv. Powder Technol. 20* (2009) 366-370.
[110] A. Ajbar, K. Alhumazi, M. Asif, Improvement of the Fluidizability of Cohesive Powders through Mixing with Small Proportions of Group A Particles, *Can. J. Chem. Eng. 83* (2005) 930-943.
[111] H. Li, R. Legros, C. M. H. Brereton, J. R. Grace, J. Chaouki, Hydrodynamic behaviour of aerogel powders in high-velocity fluidized beds, *Powder Technol. 60* (1990) 121-129.
[112] T. Zhou, H. Li, Estimation of agglomerate size for cohesive particles during fluidization, *Powder Technol. 101* (1999) 57-62.
[113] H. Li, R. Hong, Z. Wang, Fluidizing ultrafine powders with circulating fluidized bed, *Chem. Eng. Sci. 54* (1999) 5609-5615.
[114] J. A. Quevedo, R. Pfeffer, In Situ Measurements of Gas Fluidized Nanoagglomerates, *Ind. Eng. Chem. Res. 49* (2010) 5263-5269.
[115] J. M. Valverde, M. A. S. Quintanilla, A. Castellanos, P. Mills, The settling of fine cohesive powders, *EPL 54* (2001) 329.
[116] X. S. Wang, V. Palero, J. Soria, M. J. Rhodes, Laser-based planar imaging of nano-particle fluidization: Part I-determination of aggregate size and shape, *Chem. Eng. Sci.* 61 *(2006) 5476-5486.*
[117] X. S. Wang, V. Palero, J. Soria, M. J. Rhodes, Laser-based planar imaging of nano-particle fluidization: Part II-mechanistic analysis of nanoparticle aggregation, *Chem. Eng. Sci. 61* (2006) 8040-8049.
[118] J. M. Valverde, A. Castellanos, Fluidization of nanoparticles: A simple equation for estimating the size of agglomerates, *Chem. Eng. J. 140* (2008) 296-304.
[119] P. M. Jenneson, O. Gundogdu, In situ x-ray imaging of nanoparticle agglomeration in fluidized beds, *Appl. Phys. Lett. 88* (2006) 034103-3.
[120] O. Gundogdu, P. Jenneson, U. Tuzun, Nano particle fluidisation in model 2-D and 3-D beds using high speed X-ray imaging and microtomography, *J. Nanopart. Res. 9* (2007) 215-223.
[121] Y. Iwadate, M. Horio, Prediction of agglomerate sizes in bubbling fluidized beds of group C powders, *Powder Technol. 100* (1998) 223-236.
[122] T. Zhou, H. Li, Force balance modelling for agglomerating fluidization of cohesive particles, *Powder Technol. 111* (2000) 60-65.
[123] A. Castellanos, , J. M. Valverde, M. A. S. Quintanilla, Physics of Compaction of Fine Cohesive Particles, *Phys. Rev. Lett. 94* (2005) 075501.
[124] J. M. Valverde, A. Castellanos, Fluidization of nanoparticles: A modified Richardson-Zaki Law, *AIChE J. 52* (2006) 838-842.
[125] T. A. Witten, L. M. Sander, Diffusion-Limited Aggregation, a Kinetic Critical Phenomenon, *Phys. Rev. Lett. 47* (1981) 1400.
[126] J. M. Valverde, M. A. S. Quintanilla, A. Castellanos, D. Lepek, J. Quevedo, R. N. Dave, R. Pfeffer, Fluidization of fine and ultrafine particles using nitrogen and neon as fluidizing gases, *AIChE J. 54* (2008) 86-103.
[127] H. Rumpf, Zur Theorie der Zugfestigkeit vom Agglomeraten bei Kraftubertragung an Kontaktpunkten, *Chemie Ingenieur Technik 42* (1970) 538-542.
[128] J. R. Wank, S. M. George, A. W. Weimer, ALD of aluminum films on nanosized boron nitride particles in a fluidized bed, *AIChE annual meeting,* San Francisco, CA, USA (2003).
[129] B. Esmaeili, J. Chaouki, C. Dubois, Encapsulation of nanoparticles by polymerization compounding in a gas/solid fluidized bed reactor, *AIChE J. 55* (2009) 2271-2278.
[130] K. Nishii, Y. Itoh, N. Kawakami, M. Horio, A pressure swing granulation, A novel binderless granulation by cyclic fluidization and gas flow compaction, *Powder Technol. 74* (1993) 1-6.
[131] S. Matsuda, H. Hatano, A. Tsutsumi, Ultrafine particle fluidization and its application to photocatalytic NOx treatment, *Chem. Eng. J. 82* (2001) 183-188.
[132] M. Corris, B. Caussat, A. Ayral, J. Durand, Y. Kihn, P. Kalck and P. Serp, Carbon nano-tubes produced by fluidized bed catalytic CVD: first approach of the process, *Chem. Eng. Sci. 58* (2003) 4475-4482.
[133] W. Qian, F. Wei, Z. Wang, T. Liu, H. Yu, G. Luo, L. Xiang, X. Deng, Production of carbon nano-tubes in a packed bed and fluidized bed, *AIChE J. 49* (2003) 619-625.
[134] D. Geldart, A. C. Y. Wong, Fluidization of powders showing degrees of cohesiveness-I. Bed expansion, *Chem. Eng. Sci. 39* (1984) 1481-1488.
[135] L. Massimilla, G. Donsì, C. Zucchini, The structure of bubble-free gas fluidized beds of fine fluid cracking catalyst particles,

Chem. Eng. Sci. 27 (1972) 2005-2015.
[136] P. Lettieri, D. Newton, J. G. Yates, Homogeneous bed expansion of FCC catalysts, influence of temperature on the parameters of the Richardson-Zaki equation, *Powder Technol. 123* (2002) 221-231.
[137] K. Godard, J. F. Richardson, The Behaviour of Bubble-Free Fluidized Beds, *I. Chem. E. Sym. Ser. 30* (1968) 126-135.

Authors' information

Department of Chemical Engineering,
Ecole Polytechnique de Montreal,
P.O. Box 6079, Station Centre-Ville,
Montreal, Quebec,
Canada, H3C 3A7.

Jaber Shabanian was born in Babol (Iran) 1984. He gained his B.S. degree in Chemical Engineering, Petrochemical Engineering, from Isfahan University of Technology in 2006. He then received his M.Sc. degree in Chemical Engineering, Process Modeling, Simulation and Control, in Sharif University of Technology in 2009. He is currently a Ph.D. candidate in Chemical Engineering Department, Ecole Polytechnique de Montreal, working on the influence of interparticle forces on the hydrodynamics of gas-solid fluidized bed.
E-mail: jaber.shabanian@polymtl.ca

Rouzbeh Jafari was born in Tehran (Iran) 1978. He gained his B.S. degree in Chemical Engineering from Iran university of science and technology (IUST) at 2000. He received his M.Sc. degree in Chemical Engineering from Tehran university in 2003 and his Ph.D. in chemical engineering from Ecole polytechnique Montreal in 2010. He is currently a Post-Doc researcher in Chemical Engineering Department, Ecole Polytechnique de Montreal, working on Mixing, Fluidization, Process development, gasification and combustion.
E-mail: rouzbeh.jafari@polymtl.ca

Jamal Chaouki (Corresponding author) is full professor of Chemical Engineering. Jamal Chaouki obtained his engineering degree from ENSIC in Nancy, France in 1980 and Ph.D. degree from Polytechnique, Montreal. He was also post-doc fellow at UBC Vancouver from 1985 to 1986. He is now supervising 30 researchers (22 Ph.Ds, 4 PDFs, 3 research associates and 1 researcher). He is a member of the Board of the Ecole Polytechnique and several companies. He is consultant for at least 20 national and international companies. He is Principal Chaire Holder of NSREC-Total Group in hydrodynamic modeling of multiphase processes at extreme conditions.
Tel: +1-514-340-4711 X 4034
Fax: +1-514-340-4159
E-mail: jamal.chaouki@polymtl.ca